

Verifying Quantum Circuits with Level-Synchronized Tree Automata

PAROSH AZIZ ABDULLA, Uppsala University, Sweden

YO-GA CHEN, Academia Sinica, Taiwan

YU-FANG CHEN, Academia Sinica, Taiwan

LUKÁŠ HOLÍK, Brno University of Technology, Czechia and Aalborg University, Denmark

ONDREJ LENGAL, Brno University of Technology, Czechia

JYUN-AO LIN, National Taipei University of Technology, Taiwan

FANG-YI LO, Academia Sinica, Taiwan

WEI-LUN TSAI, Academia Sinica, Taiwan

We present a new method for the verification of quantum circuits based on a novel symbolic representation of sets of quantum states using *level-synchronized tree automata* (LSTAs). LSTAs extend classical tree automata by labeling each transition with a set of *choices*, which are then used to synchronize subtrees of an accepted tree. Compared to the traditional tree automata, LSTAs have an incomparable expressive power while maintaining important properties, such as closure under union and intersection, and decidable language emptiness and inclusion. We have developed an efficient and fully automated symbolic verification algorithm for quantum circuits based on LSTAs. The complexity of supported gate operations is at most quadratic, dramatically improving the exponential worst-case complexity of an earlier tree automata-based approach. Furthermore, we show that LSTAs are a promising model for *parameterized verification*, i.e., verifying the correctness of families of circuits with the same structure for any number of qubits involved, which principally lies beyond the capabilities of previous automated approaches. We implemented this method as a C++ tool and compared it with three symbolic quantum circuit verifiers and two simulators on several benchmark examples. The results show that our approach can solve problems with sizes orders of magnitude larger than the state of the art.

CCS Concepts: • **Hardware** → **Quantum computation**; • **Theory of computation** → **Tree languages**; • **Software and its engineering** → **Formal software verification**.

Additional Key Words and Phrases: quantum circuits, tree automata, verification

ACM Reference Format:

Parosh Aziz Abdulla, Yo-Ga Chen, Yu-Fang Chen, Lukáš Holík, Ondrej Lengal, Jyun-Ao Lin, Fang-Yi Lo, and Wei-Lun Tsai. 2025. Verifying Quantum Circuits with Level-Synchronized Tree Automata. *Proc. ACM Program. Lang.* 9, POPL, Article 32 (January 2025), 31 pages. <https://doi.org/10.1145/3704868>

1 Introduction

With the recent progress in quantum hardware and the push to achieve *quantum supremacy* (cf., e.g., [8]), the vision of quantum computing, an ability to solve practical conventionally unsolvable

Authors' Contact Information: [Parosh Aziz Abdulla](#), Uppsala University, Uppsala, Sweden, parosh@it.uu.se; [Yo-Ga Chen](#), Academia Sinica, Taipei, Taiwan, googagagaga@gmail.com; [Yu-Fang Chen](#), Academia Sinica, Taipei, Taiwan, gulu0724@gmail.com; [Lukáš Holík](#), Brno University of Technology, Brno, Czechia and Aalborg University, Aalborg, Denmark, holik@fit.vutbr.cz; [Ondrej Lengal](#), Brno University of Technology, Brno, Czechia, lengal@fit.vutbr.cz; [Jyun-Ao Lin](#), National Taipei University of Technology, Taipei, Taiwan, jalin@ntut.edu.tw; [Fang-Yi Lo](#), Academia Sinica, Taipei, Taiwan, lofangyi@gmail.com; [Wei-Lun Tsai](#), Academia Sinica, Taipei, Taiwan, alan23273850@gmail.com.

Permission to make digital or hard copies of all or part of this work for personal or classroom use is granted without fee provided that copies are not made or distributed for profit or commercial advantage and that copies bear this notice and the full citation on the first page. Copyrights for third-party components of this work must be honored. For all other uses, contact the owner/author(s).

© 2025 Copyright held by the owner/author(s).

ACM 2475-1421/2025/1-ART32
<https://doi.org/10.1145/3704868>

problems, is slowly getting real. Systems and languages for programming quantum computers are being intensively developed [5, 28, 56], together with efficient quantum algorithms for solving real-world problems such as machine learning [12, 21], optimization [42],

This progress drives a demand for tools for reasoning about quantum programs. Writing quantum programs is indeed immensely challenging due to their probabilistic nature and the exponential size of the computational space. Errors are easily made and difficult to find. Tools for reasoning about quantum programs would ideally have the following properties: (1) *Flexibility*: allows flexible specification of properties of interest, (2) *Diagnostics*: provides precise bug diagnostics, (3) *Automation*: operates automatically, and (4) *Scalability*: scales efficiently to verify useful programs.

Symbolic verification [4, 14, 35, 36, 43] is one of the most successful techniques that satisfies the above criteria for conventional programs. However, there has been minimal progress in the area of symbolic verification for quantum circuits. This paper contributes towards filling this gap by adapting automata-based symbolic verification [4] to quantum circuits. More specifically, we think of the symbolic verification problem in terms of Hoare triples $\{P\} C \{Q\}$, where P and Q are sets of quantum states representing the *pre-condition* and the *post-condition*, and C is a quantum circuit. We aim to use symbolic verification to check the *validity* of the triple, ensuring that all executions of C from states in P result in states within Q .

Example 1. As an example of a verification problem, let C be the circuit creating Bell states in Fig. 1. The circuit begins by applying the H gate to the first qubit, followed by a controlled- X gate with the first qubit as the control and the second qubit as the target. The circuit converts 2-qubit computational basis states to Bell states (maximally entangled states). Its correct implementation satisfies the Hoare triple with the pre-condition $P = \{|00\rangle, |01\rangle, |10\rangle, |11\rangle\}$ (computational basis states are denoted using the Dirac notation $|x_1 x_2\rangle$) and the post-condition $Q = \{\frac{1}{\sqrt{2}}(|00\rangle \pm |11\rangle), \frac{1}{\sqrt{2}}(|01\rangle \pm |10\rangle) \mid \pm \in \{+, -\}\}$ (Bell states). \square

Our quantum circuit symbolic verification framework comprises three major components: (1) a *succinct symbolic representation of sets of quantum states* allowing efficient manipulation and facilitating flexible specification of desired pre- and post-conditions, (2) algorithms for *symbolic execution of individual quantum gates*, which compute the symbolic representation of output states from input states and explore the reachable state space after circuit execution, (3) *entailment test* on the symbolic representation to verify that all reachable states conform to the specified post-condition or report a witness when the specification is violated. Together, these components enable *flexible, diagnostic, automated, and scalable* verification of quantum circuits.

Succinct symbolic representation. The central part of our framework is a novel symbolic representation of sets of quantum states, the *level-synchronized tree automata (LSTAs)*. The concept evolved from decision diagrams that have been used to succinctly represent one quantum state, e.g., in [41, 48, 50, 53]. They are based on viewing a quantum state as a binary tree, where each branch (a path from a root to a leaf) represents a *computational basis state*, such as $|10\rangle$ or $|00\rangle$ for a two-qubit circuit. The tree is *perfect*, i.e., the length of every branch is the same and equals the number of qubits in the circuit. The leaves represent the *complex probability amplitudes*¹ of the

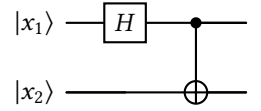


Fig. 1. The Bell state circuit. \bullet denotes the control qubit and \oplus denotes the target qubit on which X is applied.

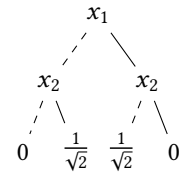


Fig. 2. $\frac{1}{\sqrt{2}}(|01\rangle + |10\rangle)$.

¹Amplitude is a generalization of the concept of “probability.” The square of the absolute value of a complex amplitude represents the corresponding probability. The use of complex numbers allows for the expression of “negative probabilities” (obtained after squaring) that are canceled out due to interference.

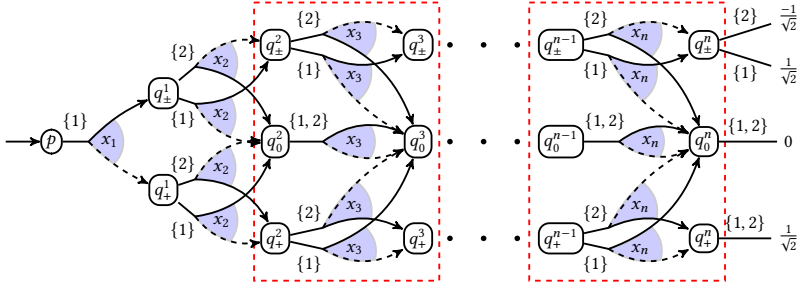


Fig. 4. An LSTA representing the set of quantum states of the form $\frac{1}{\sqrt{2}}(|0b_2b_3 \dots b_n\rangle \pm |1\bar{b}_2\bar{b}_3 \dots \bar{b}_n\rangle)$.

state. An example in Fig. 2 shows the tree representing a state with two qubits where the basis states $|01\rangle$ and $|10\rangle$ have the probability amplitude $\frac{1}{\sqrt{2}}$ and the others have the amplitude 0. In the figure, dashed edges denote the 0 value and solid edges denote the 1 value of the variable that is in the source node of the edge, so the $|01\rangle$ state is encoded by first taking the dashed edge (from the node labelled by x_1) and then the solid one (from the left-most x_2 node).

LSTAs enrich decision diagrams with three important features. First, they allow *disjunctive branching*, which increases their compactness, enabling different quantum states to share common structures. This has also been observed and used in the work of [19], resulting in an exponential space saving compared with storing quantum states as a set of BDDs. Second, they allow *cycles*, which enables representing unboundedly many quantum states and opens a path towards verification of quantum circuits with a parameterized number of qubits. The addition of cycles and disjunctive branching results in a class of tree automata. On top of that, LSTAs are equipped with a novel mechanism of *tree level synchronization*, which yet again dramatically increases succinctness (up to exponentially) and simplifies the symbolic execution of quantum gates.

Example 2 (An LSTA for a simple 2-qubit circuit.). We intuitively explain the features of LSTAs on an encoding of the post-condition from Example 1. The set of Bell states (post-condition) is generated by the LSTA in Fig. 3. The LSTA generates trees representing quantum states from the root downward, starting at the root state p , and proceeding iteratively by picking a transition to generate children states, until reaching the leaves. For example, the tree from Fig. 2 can be generated by first picking the

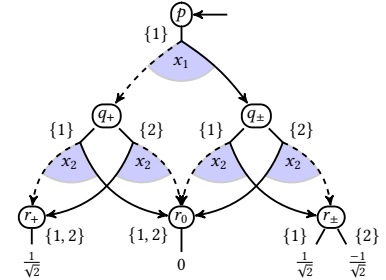


Fig. 3. The LSTA representing Bell states

transition $(p \xrightarrow{\{1\}} x_1 \xrightarrow{\{1\}} q_+)$, then the two transitions, $(q_+ \xrightarrow{\{2\}} x_2 \xrightarrow{\{1,2\}} r_+)$, $(q_+ \xrightarrow{\{2\}} x_2 \xrightarrow{\{1,2\}} r_-)$, and ending with the leaf transitions $(r_+ \xrightarrow{\{1,2\}} \frac{1}{\sqrt{2}})$, $(r_0 \xrightarrow{\{1,2\}} 0)$, $(r_- \xrightarrow{\{1,2\}} \frac{1}{\sqrt{2}})$. Like the traditional *tree automata* (TAs) model [23], LSTAs allow disjunctive branches and use them to express multiple states with a shared structure. Here, the states q_+ , q_- , and r_\pm have two disjunctive transitions. Their combination would generate 8 different trees. Not all of these combinations are, however, intended. LSTAs enrich the traditional TA model by labeling the transitions with sets of *choices* (the $\{1\}$, $\{2\}$, and $\{1, 2\}$ in this example). The choices play an essential role in restricting the set of generated trees to the intended ones. Namely, at every tree level, the used transitions must agree on a common choice, otherwise the tree will be rejected. Particularly in the second level of the tree, the transitions labeled $\{1\}$ can be taken together, as they agree on 1, or transitions labeled $\{2\}$ can be taken together, as they agree on 2. A combination

of a transition labeled $\{1\}$ and a transition labeled $\{2\}$ is not admissible as their sets of choices are disjoint. Including also the admissible choices at the third level, the LSTA generates exactly the 4 Bell states (using the 9 transitions in the figure). \square

Example 3 (Succinctness of LSTAs in a larger n -qubit circuit). The succinctness of LSTAs and the role of the level synchronization is visible when the previous example is generalized to n qubits, where LSTAs can represent the 2^n output quantum states with a *linear number of transitions*. Indeed, the 2-qubit circuit can be generalized to n -qubit circuits, generating the so-called GHZ states² $Q = \{\frac{1}{\sqrt{2}}(|0b_2b_3 \dots b_n\rangle \pm |1\bar{b}_2\bar{b}_3 \dots \bar{b}_n\rangle) \mid b_2b_3 \dots b_n \in \mathbb{B}^{n-1} \wedge \pm \in \{+, -\}\}$, where \bar{b} denotes the complement of b . We visualize a GHZ state in Fig. 5; the basis $|0b_2b_3 \dots b_n\rangle$ has amplitude $\frac{1}{\sqrt{2}}$ and $|1\bar{b}_2\bar{b}_3 \dots \bar{b}_n\rangle$ has amplitude $\frac{1}{\sqrt{2}}$ or $\frac{-1}{\sqrt{2}}$. An LSTA can be used to represent the post-condition Q with only $5n - 1$ transitions (see Fig. 4). This results in an *exponential space saving* compared to other standard ways

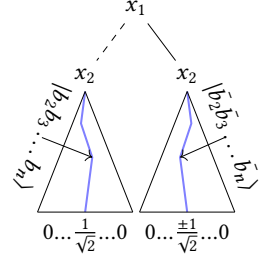


Fig. 5. GHZ states

of storing sets of quantum states precisely, such as traditional tree automata [19], sets of BDDs [50], or sets of state vectors [37], which all need exponential space to store the 2^n quantum states in Q .

LSTAs achieve this succinctness by combining disjunctive branching and level synchronization. Each GHZ state consists of a left-hand side 0-rooted subtree (called 0-subtree below) and a right-hand side 1-rooted subtree (called 1-subtree), see Fig. 5. Each subtree has all leaves except one labeled 0. The two distinguished leaves are reached by two paths that are mirror images of each other, representing the 0-basis $b_2b_3 \dots b_n$ and the inverted 1-basis $\bar{b}_2\bar{b}_3 \dots \bar{b}_n$. Disjunctive branching does the first part of the job: it represents the set of all 2^{n-1} subtrees with a single distinguished leaf by a number of transitions linear to n . The LSTA traces the path towards the distinguished leaf by a sequence of states q_+^1, \dots, q_+^n in the 0-subtree and q_-^1, \dots, q_-^n in the 1-subtree (Fig. 4). When the subtrees are generated, each state on the path spawns two children. One is the next state in the sequence, the other is a state q_0^i that generates a uniform tree with all leaves 0. Each state on the path can choose to continue the path to the left or to the right by choosing one of two transitions (this is the disjunctive branching).

Level synchronization is then used to ensure that the two paths towards the distinguished leaves are mirror images of each other. In every level of the tree, if the path in the 0-subtree is continuing to the left, then the path in the 1-subtree must continue to the right, and vice versa. The LSTA in Fig. 4 achieves this as follows: in the 0-subtree, the left/right transitions continuing the path are associated with the choices 1 and 2, respectively, and in the right subtree, the left/right continuing transitions are associated with the choices in the inverted manner, 2 and 1, respectively. Without this level-synchronization mechanism, each 0-subtree would need a unique root transition to connect to its corresponding 1-subtree, requiring 2^{n-1} root transitions (we argue in Theorem 16 that an exponential number of transitions is unavoidable). \square

In fact, many quantum gates create a correspondence between subtrees of a tree (cf. Section 2.2.1 and Fig. 7)—this is a typical manifestation of quantum entanglement. Hence, level synchronization is also helpful in the general case, not only for some special circuits. We will give more examples in Section 4, where we demonstrate that LSTAs can succinctly express a wide range of correctness properties of quantum circuits, including the following verification tasks. All the involved LSTAs are of a size linear in the number of qubits.

²Often GHZ states refer to the set $\{\frac{1}{\sqrt{2}}(|0^n\rangle + |1^n\rangle) \mid n \in \mathbb{N}\}$, but here we refer to a generalized version obtained by feeding all n -qubit computational basis states to the GHZ generating circuit.

- We can verify the correctness of a circuit component, for example, *a multi-control Toffoli gate implemented with standard Toffoli gates (with two control inputs)*.
- We can construct a template oracle circuit that reads secret strings from the input and use it to verify *oracle-based circuits*. E.g., by verifying a Bernstein-Varzirani circuit against all possible oracles, we ensure it correctly identifies the secret string with just one oracle query.
- By allowing the use of variables at tree leaves, we can verify that *a Grover iteration indeed increases the probability of finding a correct solution* for infinitely many feasible input states.
- Moreover, LSTAs can be used to specify *the equivalence of two circuits C and C'* . We can use LSTAs to express a set of 2^n *linearly independent vectors* compactly using a linear (in n) number of transitions. If we use this LSTA as the pre-condition and also as the post-condition for a symbolic verification framework, we can check if a circuit's function corresponds to *identity*. We can then check if C and C' are equivalent by sequentially composing C with the inverse of C' and checking if the result is identity.

Fast symbolic execution of gates. With an LSTA-encoded precondition, the next step is to compute an LSTA encoding all states reachable from the precondition after executing a circuit. In Section 5, we develop algorithms to execute gates symbolically, i.e., to compute LSTA-represented output states from LSTA-represented input states and a single quantum gate U . We support a wide variety of quantum gates, including all single-qubit gates and (multi-)control gates, such as the Toffoli gate. We show that all supported gates can be executed over LSTAs in a time *quadratic* in the size of the input LSTA. The reachable states can then be computed via a sequence of symbolic gate executions.

Entailment of LSTAs and other operations. The next step is to verify if all reachable states satisfy the postcondition. In Section 6, we present an algorithm for the entailment (i.e., language inclusion) test between LSTAs. We show that LSTA entailment is decidable with the complexity between **PSPACE** and **EXSPACE** and can be implemented to run fast enough in practice. When the entailment test fails, the algorithm can return a tree witnessing the entailment violation. The quantum state represented by the tree can then be used to diagnose the quantum circuit and find out why verification fails. We also show that LSTAs have decidable (**PSPACE**-complete) emptiness problem, are closed under union and intersection, but not closed under complement.

Experimental evaluation. Our experimental results in Section 7 clearly demonstrate that LSTAs enable a highly efficient and scalable framework for automated quantum circuit verification. Implemented as an updated version of our tool, AUTOQ, our approach successfully handled multiple verification tasks, verified all specified correctness properties, and found all injected bugs. We compared the new AUTOQ with three recent symbolic quantum circuit verifiers, AUTOQ-OLD [19], CAAL [20], and symQV [9] and two simulators SLIQSIM [50] and SV-SIM [37] on several benchmark examples. Notably, AUTOQ significantly outperformed all other tools in these tasks.

Towards parameterized verification of quantum circuit. As LSTAs naturally allow cycles in their transition relation, they show a promise for *parameterized verification* of quantum circuits, checking the correctness of a *circuit template* for any (parametric) number of qubits. For instance, Fig. 6 contains an LSTA that encodes the set of states $|0^n\rangle$ for any number of qubits n . Here, we label transitions with x to denote that it is an unspecified qubit, and its value depends on the tree level on which it is used. We extended our approach to support various types of parameterized quantum gates, including the application of CX gates to every consecutive qubit. We were able to describe the template and establish the correctness

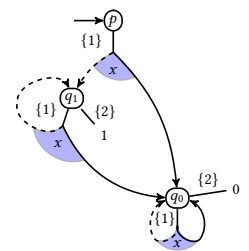


Fig. 6. $\{|0^n\rangle \mid n \geq 1\}$.

of GHZ circuits [29] and circuits performing *diagonal Hamiltonian simulation* [40] and *fermionic unitary evolution* [59], which are frequently used in quantum chemistry and material science.

2 Preliminaries

This section aims to provide readers with a basic understanding of quantum computing. Quantum computers are programmed through *quantum gates*, and each gate application updates the global *quantum state*. A *quantum circuit* is a sequence of quantum gate applications.

2.1 Quantum States

In a traditional computer system with n bits, a state is represented by n Boolean values. In the quantum world, such states are referred to as *computational basis states*. For example, in a system with three bits labeled x_1, x_2 , and x_3 , the computational basis state $|011\rangle$ indicates that the value of x_1 is 0 and the values of x_2 and x_3 are 1. In a quantum system, an n -qubit *quantum state* encodes the amplitude information of a superposition of all possible n -bit computational basis states, denoted as a formal sum $\sum_{j \in \{0,1\}^n} a_j \cdot |j\rangle$, where $a_0, a_1, \dots, a_{2^n-1} \in \mathbb{C}$ are *complex amplitudes* satisfying the property that $\sum_{j \in \{0,1\}^n} |a_j|^2 = 1$. Intuitively, $|a_j|^2$ is the probability that when we measure the quantum state in the computational basis, we obtain the classical state $|j\rangle$; these probabilities must sum up to 1 for all computational basis states. The standard representation of a quantum state is a vector $(a_0, a_1, \dots, a_{2^n-1})^T$ of amplitude values, where the superscript T denotes *transposition*.

We represent a quantum state using a *decision tree* where each branch represents a computational basis state and the leaves hold complex amplitudes. We demonstrate in Fig. 8a an example of a decision tree encoding a quantum state $q = a \cdot |00\rangle + b \cdot |01\rangle + c \cdot |10\rangle + d \cdot |11\rangle$. This viewpoint enables us to see the definition of standard quantum gate operations as tree transformations.³ The viewpoint also allows us to represent a set of states compactly using LSTAs. In fact, the tree view can be generalized to handle any vector of 2^n entries. We will show that LSTAs can compactly represent some sets of linearly independent vectors and use them for testing circuit equivalence.

2.2 Quantum Gates and Circuits

The two main types of quantum gates used in state-of-the-art quantum computers are *single-qubit gates* and *controlled gates*.

2.2.1 General single-qubit gates. In general, a single-qubit gate is presented as a *unitary complex matrix* U , shown below together with some common examples of this category (θ is a parameter):

$$U = \begin{pmatrix} u_1 & u_2 \\ u_3 & u_4 \end{pmatrix}, X = \begin{pmatrix} 0 & 1 \\ 1 & 0 \end{pmatrix}, Y = \begin{pmatrix} 0 & -i \\ i & 0 \end{pmatrix}, R_X(\theta) = \begin{pmatrix} \cos \frac{\theta}{2} & -i \sin \frac{\theta}{2} \\ -i \sin \frac{\theta}{2} & \cos \frac{\theta}{2} \end{pmatrix}, H = \frac{1}{\sqrt{2}} \begin{pmatrix} 1 & 1 \\ 1 & -1 \end{pmatrix},$$

$$Z = \begin{pmatrix} 1 & 0 \\ 0 & -1 \end{pmatrix}, S = \begin{pmatrix} 1 & 0 \\ 0 & i \end{pmatrix}, T = \begin{pmatrix} 1 & 0 \\ 0 & e^{\frac{i\pi}{4}} \end{pmatrix}, R_Z(\theta) = \begin{pmatrix} e^{-\frac{i\theta}{2}} & 0 \\ 0 & e^{\frac{i\theta}{2}} \end{pmatrix}, \text{Ph}(\theta) = \begin{pmatrix} e^{i\theta} & 0 \\ 0 & e^{i\theta} \end{pmatrix}.$$

We use U_i to denote the application of gate U to the i -th qubit. In linear algebra, the application of a gate to a state $(a_0, a_1, \dots, a_{2^n-1})^T$ corresponds to the matrix multiplication $(I_{i-1} \otimes U \otimes I_{n-i}) \cdot (a_0, a_1, \dots, a_{2^n-1})^T$, where I_j is the 2^j dimensional identity matrix and \otimes is the *tensor product*. Under the tree view, a gate operation corresponds to a tree transformation on every two neighboring subtrees at level i . We use Fig. 7 to illustrate how the transformation U_3 works. Here T_0 and T_1 are the 0-subtree and 1-subtree of a

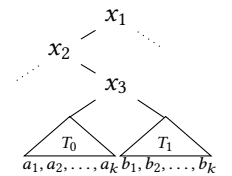


Fig. 7. T_0 and T_1

³Note that we do not discuss how to represent complex numbers; representing complex numbers precisely in computers is an orthogonal issue to our work and can be handled by, e.g., the approach from [62] and [50].

node labeled x_3 . Their leaves encode the amplitudes a_1, a_2, \dots, a_k and b_1, b_2, \dots, b_k , respectively. After applying U_3 , the leaves of T_0 become $(u_1 \cdot a_1 + u_2 \cdot b_1), (u_1 \cdot a_2 + u_2 \cdot b_2), \dots, (u_1 \cdot a_k + u_2 \cdot b_k)$, obtained by multiplying the amplitudes of T_0 with u_1 , those of T_1 with u_2 , and summing up the two. Similarly, the leaves of T_1 become $(u_3 \cdot a_1 + u_4 \cdot b_1), (u_3 \cdot a_2 + u_4 \cdot b_2), \dots, (u_3 \cdot a_k + u_4 \cdot b_k)$. The same transformation occurs in all neighboring subtrees at the same level. It is essential to note that the sum of probabilities remains the same after the U gate application, as U is unitary. We provide examples of applying X_2, Z_2, H_1 on q in Fig. 8b, Fig. 8c, and Fig. 8d, respectively.

2.2.2 Two frequently used sub-categories.

In fact, most of the quantum gates have a simpler structure than the general case. Except the $R_X(\theta)$ and H gates, all other considered single-qubit gates belong to the

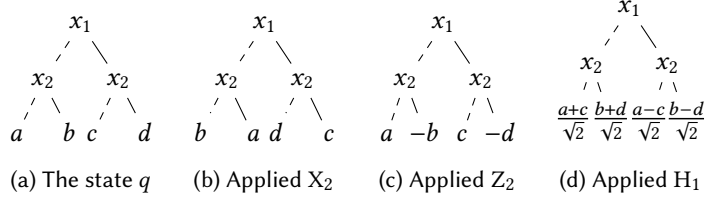


Fig. 8. The effect of applying single-qubit quantum gates to the state q .

following two categories (or their composition): (1) the X (negation) gate and (2) diagonal matrix ($u_2 = u_3 = 0$) gates. This allows more efficient automata algorithms than the general case.

The X gate is the quantum “negation” gate. Applying X_i on a quantum state effectively swaps the 0- and 1-branches of all nodes at the level i . An example of applying X_2 on q is available at Fig. 8b.

Gates with diagonal matrices, e.g., $Z, S, T, R_Z(\theta)$, and $\text{Ph}(\theta)$, multiply all 0- or 1-subtrees under nodes labeled x_i by the complex values r_0 and r_1 , respectively. We note that $|r_0|$ and $|r_1|$ always equal 1. We use D^{r_0, r_1} to denote a gate with the diagonal matrix $D^{r_0, r_1} = \begin{pmatrix} r_0 & 0 \\ 0 & r_1 \end{pmatrix}$. We refer the reader to Fig. 8c for an example of the application of $Z_2 = D_2^{1, -1}$ on q . Gates with anti-diagonal matrices, e.g., Y , can be composed from X and $D^{i, -i}$ (i.e., $Y = X \cdot D^{i, -i}$).

2.2.3 Controlled gates. A controlled gate CU uses another quantum gate U as its parameter. CU has a control qubit x_c and the gate U is applied only when the control qubit x_c has value 1. The controlled X gate CX_2^1 has the control qubit x_1 and would apply X_2 when x_1 is valued 1.

The result of applying CX_2^1 on q is available in Fig. 9b. Observe that X_2 is only applied to the 1-subtree of x_1 . On the other hand, the result of applying CX_1^2 on q is available in Fig. 9c. Observe that all 0-subtrees at level 2 remain the same as in q , but the 1-subtrees at level 2 are updated to the corresponding ones after applying the X_1 gate to q .

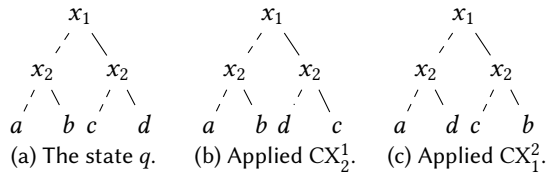


Fig. 9. The effect of applying controlled gates to the state q .

2.2.4 Quantum circuits. As we mentioned before, a quantum circuit is a sequence of quantum gates. Executing a circuit effectively performs a sequence of tree updates following the gates’ semantics. We often represent a quantum circuit using a diagram as in Fig. 1, which is also written as $H_1CX_2^1$.

As an analogy, in classical circuits, a state corresponds to a computational basis state, and a gate application transforms one basis state to another. This process can be represented using a single tree branch. In contrast, encoding quantum states requires accounting for the amplitude values of all computational basis states, which necessitates using a complete tree structure for representation. Our method captures key quantum-specific features, particularly the ability to encode superpositions of basis states and their associated amplitudes. While our methods can be adapted to verify classical circuits by simplifying the state representation and adding support to

classical gates, the primary distinction lies in our approach to handling quantum superposition and gate semantics—features that are absent in classical computation.

3 Level-Synchronized Tree Automata

In this paper, a new tree automata model called *Level-Synchronized Tree Automata* (LSTAs) is developed. The expressiveness of this model is incomparable with the traditional tree automata model (Theorem 17) while maintaining important properties such as being closed under union and intersection. It also allows for testing language emptiness and inclusion, enabling the testing of whether all reachable states are included in the post-condition. One crucial advantage of LSTAs is that they annotate transitions with “choices” and use them to coordinate between tree branches, enabling efficient quantum state encoding and gate operations (see Section 2.2).

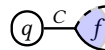
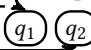
3.1 Formal Definition of LSTAs

Binary Trees. We use \mathbb{N} to represent the set of natural numbers (without 0), $\mathbb{N}_0 = \mathbb{N} \cup \{0\}$ to represent the set of non-negative integers, and $\mathbb{B} = \{0, 1\}$ to represent the Boolean values. A ranked alphabet is a set of symbols Σ with a corresponding rank given by a function $\# : \Sigma \rightarrow \{0, 2\}$. The symbols with rank 0 are called *leaf* symbols, and those with rank 2 are called *internal* symbols.

A *binary tree* is a finite map $T : \{0, 1\}^* \rightarrow \Sigma$ that maps *tree nodes* (i.e., words over the alphabet $\{0, 1\}$) to symbols in Σ , and satisfies that (1) the domain of T is *prefix-closed* and (2) if $T(v) = f$ and f is internal, then the set of *children* of v in T is $\{v.0, v.1\}$, and if f is a leaf symbol then v has no children. Nodes labeled by leaf symbols and internal symbols are called *leaf nodes* and *internal nodes*, respectively. A node’s *height* is its word length, denoted $\text{ht}(w)$; e.g., $\text{ht}(01010) = 5$. A node w is at tree level i when $\text{ht}(w) = i$. A tree is *perfect* if all leaf nodes have the same height. We need only *perfect binary trees* to represent quantum states or vectors of sizes 2^n .

Example 4. The quantum state of Fig. 2 corresponds to a tree T with $T(\epsilon) = x_1$, $T(0) = T(1) = x_2$, $T(00) = T(11) = 0$, and $T(01) = T(10) = \frac{1}{\sqrt{2}}$, where ϵ is an empty string. We have $\text{dom}(T) = \{\epsilon, 0, 1, 00, 01, 10, 11\}$. Children of the node 0 are 00 and 01. The leaf node 01 has no children.

Definition 5. A *level-synchronized tree automaton* (LSTA) is a tuple $\mathcal{A} = \langle Q, \Sigma, \Delta, \mathcal{R} \rangle$ where

- (1) Q is a finite set of *states*, $\mathcal{R} \subseteq Q$ is a set of *root states*, and Σ is a ranked alphabet.
- (2) Δ is a set of transitions of the form $q \xrightarrow{-C} f(q_1, q_2)$ (*internal trans.*) or $q \xrightarrow{-C} f$ (*leaf trans.*), where $C \subseteq \mathbb{N}_0$ is a finite set of *choices* (represented as natural numbers), $q, q_1, q_2 \in Q$, and $f \in \Sigma$. In figures, we draw internal and leaf transitions as  and .
- (3) We call q , f , C , and $\{q_1, q_2\}$ the *top*, the *symbol*, the *choices*, and the *bottom*, respectively, of the transition δ , and denote them by $\text{top}(\delta)$, $\text{sym}(\delta)$, $\ell(\delta)$, and $\text{bot}(\delta)$, respectively. We use $|\mathcal{A}|$ to denote \mathcal{A} ’s number of states.
- (4) We further require that the choices of transitions with the same top state are disjoint, i.e., $\forall \delta_1 \neq \delta_2 \in \Delta : \text{top}(\delta_1) = \text{top}(\delta_2) \implies \ell(\delta_1) \cap \ell(\delta_2) = \emptyset$

The language of an LSTA. A *run* of an LSTA \mathcal{A} on a tree T is a total map $\rho : \text{dom}(T) \rightarrow \Delta$ from tree nodes to transitions of \mathcal{A} such that for each node $v \in \text{dom}(T)$, when v is an internal node, $\rho(v)$ is of the form $q \xrightarrow{-C} T(v)(q_0, q_1)$, where the two bottom states $q_0 = \text{top}(\rho(v.0))$ and $q_1 = \text{top}(\rho(v.1))$ are the two top states of v ’s children $\rho(v.0)$ and $\rho(v.1)$. When v is a leaf node, $\rho(v)$ is of the form $q \xrightarrow{-C} T(v)$.

Example 6. We define a *run* ρ of the LSTA \mathcal{A} in Fig. 3 on the tree T in Fig. 2 as follows. We have

$$\begin{aligned} \rho(\epsilon) &= p \xrightarrow{-\{1\}} x_1(q_+, q_\pm), & \rho(0) &= q_+ \xrightarrow{-\{2\}} x_2(r_0, r_+), & \rho(1) &= q_\pm \xrightarrow{-\{2\}} x_2(r_\pm, r_0), \\ \rho(01) &= r_+ \xrightarrow{-\{1,2\}} \frac{1}{\sqrt{2}}, & \rho(10) &= r_\pm \xrightarrow{-\{1\}} \frac{1}{\sqrt{2}}, & \rho(00) &= \rho(11) = r_0 \xrightarrow{-\{1,2\}} 0. \end{aligned} \quad \square$$

We define the *level* d of a run ρ as the set of transitions with height d

$$\text{level}(\rho, d) := \{\rho(w) \mid w \in \text{dom}(T) \wedge \text{ht}(w) = d\}.$$

The run ρ is *accepting* if $\text{top}(\rho(\epsilon)) \in \mathcal{R}$ and all transitions from the same level share some common choice, i.e., $\forall d \in \mathbb{N}: \bigcap_{\delta \in \text{level}(\rho, d)} \ell(\delta) \neq \emptyset$ —in other words, transitions at each tree level are *synchronized*. The *language* of \mathcal{A} is the set $\mathcal{L}(\mathcal{A})$ of trees T with an accepting run.

Example 7. Continuing from Example 6, we have $\text{level}(\rho, 1) = \{q_+ \dashv\{2\} \rightarrow x_2(r_0, r_+), q_\pm \dashv\{2\} \rightarrow x_2(r_\pm, r_0)\}$ and $\text{level}(\rho, 2) = \{r_+ \dashv\{1,2\} \rightarrow \frac{1}{\sqrt{2}}, r_0 \dashv\{1,2\} \rightarrow 0, r_\pm \dashv\{1\} \rightarrow \frac{1}{\sqrt{2}}\}$. Observe that ρ is accepting because $\text{top}(\rho(\epsilon)) = p \in \mathcal{R}$, the transitions from $\text{level}(\rho, 1)$ have a common choice 2, and those from $\text{level}(\rho, 2)$ have a common choice 1. \square

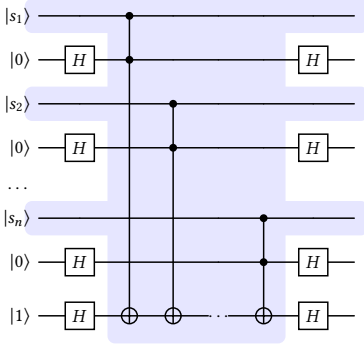
We defer a detailed discussion on properties of LSTAs to Section 6. At this point, we just note that the *inclusion test* over LSTAs, i.e., checking if $\mathcal{L}(\mathcal{A}_1) \subseteq \mathcal{L}(\mathcal{A}_2)$ for LSTAs \mathcal{A}_1 and \mathcal{A}_2 , is decidable.

4 Using LSTAs To Describe Correctness Properties

We can use an LSTA to encode a set of perfect binary trees (quantum states or vectors) and use them as pre- and post-conditions for verification of quantum circuits. Below, we will provide examples of the verification problems and the corresponding specifications given using LSTAs.

4.1 Verification of Oracle-Based Algorithms

An *oracle circuit* is a black box circuit used to encode a specific function. It plays a crucial role in many quantum algorithms by providing a way to query information in a single computational step. In the case of Grover's search algorithm [30], the oracle circuit encodes a function $f(x): \mathbb{B}^n \rightarrow \mathbb{B}$ that outputs 1 if x is the solution and 0 otherwise. In the case of the Bernstein-Vazirani algorithm [10], the oracle circuit encodes a secret bit string. To verify the correctness of these algorithms against all possible oracles, one way is to create a *parameterized* oracle circuit that uses input qubits and control gates to generate the corresponding oracle. By composing the parameterized oracle circuit and the circuit to be verified, we can create a framework to verify the correctness of these circuits against all oracles.

Taking verification of the Bernstein-Vazirani algorithm (BV) as an example, the composed circuit consists of $2n + 1$ qubits (Fig. 10), where the highlighted part  is the oracle circuit and the rest is the circuit under verification. We emphasize that in our setting, we consider parameterized oracle with the secret provided as a part of the input of the circuit. The qubits s_1, s_2, \dots, s_n serve as the input for the parameterized oracle circuit, and the other qubits act as the working tape of the circuit being verified, particularly, the last qubit acts as the ancilla, i.e., an *auxiliary variable* in the sense of classical program verification. We will verify the correctness of the implementation using the precondition $\{|s_1 0 s_2 0 \dots s_n 0 1\rangle \mid s_1, s_2, \dots, s_n \in \mathbb{B}\}$ and the postcondition $\{|s_1 s_1 s_2 s_2 \dots s_n s_n 1\rangle \mid s_1, s_2, \dots, s_n \in \mathbb{B}\}$. That is, considering all possible secret strings $s_1 s_2 \dots s_n$ as the input of the oracle circuit and verifying that the BV circuit finds the same string at the output. We show the LSTA representing the postcondition in Fig. 11. In this LSTA, the states q_0^i generate subtrees with leaves 0. From the state q^i , the LSTA picks a secret bit b using the disjunctive branch, remembers it in states q_R^{i+1}

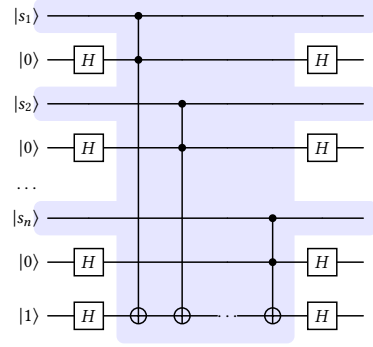


Fig. 10. BV circuit. Standard Toffoli gates have two \bullet as controls and one \oplus as the target.

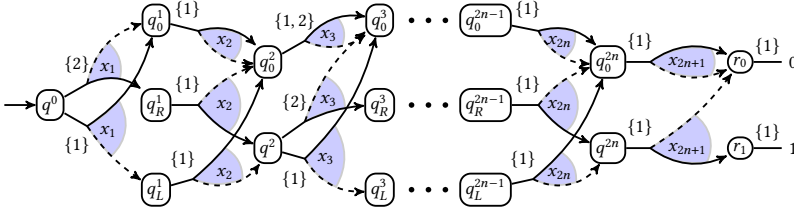


Fig. 11. An LSTA encoding the BV postcondition $|s_1 s_1 \dots s_n s_n 1\rangle$

($b = 1$) or q_L^{i+1} ($b = 0$), and repeats the value in the next transition. The precondition can be modeled in a similar manner to Fig. 11 and, hence, omitted.

4.2 Verification of Compound Multi-Control Quantum Gates

When implementing quantum algorithms on quantum computers, which have a limited set of supported gates, one often needs to find a way how to implement an unsupported gate by composing several natively supported gates. For instance, the multi-control Toffoli gate is not typically supported and is often created using standard Toffoli gates (cf. Fig. 12). In this type of circuit, qubits $|c_1\rangle, \dots, |c_n\rangle$ serve as the control, those $|0\rangle$ below the controlled qubits are the ancilla qubits, and the last qubit $|t\rangle$ is the target. For this circuit to be correct, it should hold that (1) it maps ancilla qubits $|0^{n-1}\rangle$ to $|0^{n-1}\rangle$ (we do not impose any restrictions on the behavior of the circuit if the input ancillas are not $|0^n\rangle$) and (2) the operation of the circuit on the rest of the qubits is equivalent to a multi-control Toffoli gate, i.e., for computational bases of the form $|c_1 \dots c_n t\rangle$, it swaps the amplitudes of bases $|1^n 0\rangle$ and $|1^n 1\rangle$ and keeps all the other bases the same.

A fundamental issue with specifying the functionality of such circuits using Hoare triples is that we need to express a mapping between input and output quantum states, which is not directly expressible using only sets of states⁴. In the case of multi-control gates, we can use the fact that the values of the control qubits should not change at the output, and we only care about the case the values of the ancillas remain 0, the only qubit whose value will change is the target $|t\rangle$. Hence, we reduce the verification problem to two sub-problems against the two pairs of pre- and postconditions Pre_k and Post_k below, for the value of $|t\rangle$ being $k \in \mathbb{B}$.

$$\text{Pre}_k = \{|c_1 c_2 c_3 0 \dots c_n 0 k\rangle \mid c_1, \dots, c_n \in \mathbb{B}\}$$

$$\text{Post}_k = \{|c_1 c_2 c_3 0 \dots c_n 0 k'\rangle \mid c_1, \dots, c_n \in \mathbb{B}, k' = (c_1 \wedge \dots \wedge c_n) \oplus k\}$$

Intuitively, the postcondition says that if all control qubits are set to 1, then the value of the target should be flipped (denoted using the xor operator \oplus). Pre_k and Post_k can be modelled using LSTAs in a similar way as in Fig. 11. Specification of other multi-control gates could be done likewise.

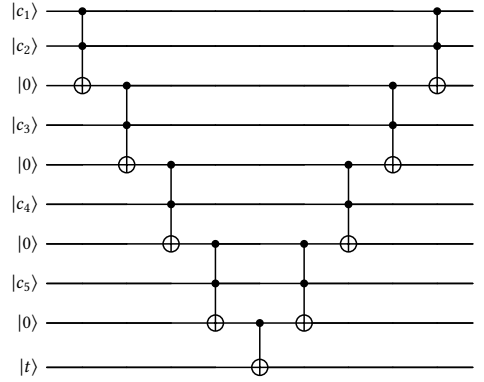
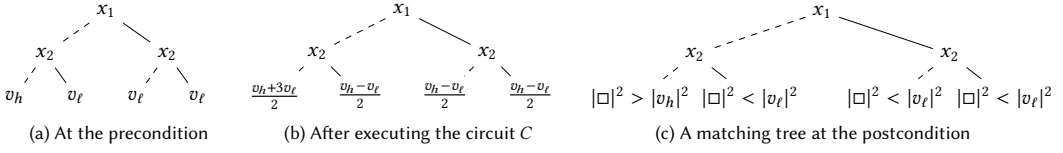


Fig. 12. Multi-control Toffoli with 5 control qubits.

⁴One could, indeed, make a copy of the input qubit values, but this would cause a blow-up in the size of the underlying representation, losing the compactness of LSTAs.

Fig. 14. Verification of a circuit C amplifying the amplitude of $|00\rangle$.

4.3 Equivalence Checking

When considering the LSTA model's expressiveness as a specification language, it is interesting to note that it can be used to express that a circuit implements the *identity* function, allowing for checking of circuit equivalence. More precisely, given two circuits C_1 and

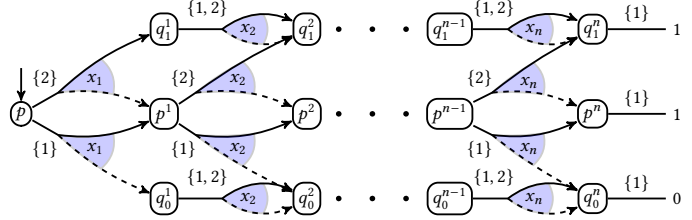


Fig. 13. LSTA for the pre- and post-condition for equivalence checking

C_2 , we can check if they are equivalent by checking if $C_1 C_2^\dagger$ is an identity, where C_2^\dagger can be obtained from C_2 by reverting it (i.e., inputs are swapped with outputs) and substituting every gate by its inverse. Since all quantum gates correspond to unitary matrices, their inverses can be obtained by taking their conjugate transpose. For instance, the inverse of a single qubit gate $U = \begin{pmatrix} u_1 & u_2 \\ u_3 & u_4 \end{pmatrix}$ is the gate $U^\dagger = \begin{pmatrix} \bar{u}_1 & \bar{u}_3 \\ \bar{u}_2 & \bar{u}_4 \end{pmatrix}$ in the same form, where \bar{u} is the complex conjugate of u (therefore, whenever we can implement the gate U , we can also obtain an implementation of the gate U^\dagger).

We can then verify if an n -qubit circuit is an identity by testing it against 2^n linearly independent *vectors* and checking if each resulting vector matches its input vector (this is due to the fact that the identity matrix is the only matrix that maps all vectors back to themselves; due to linearity, it suffices to only try a maximal set of linearly independent vectors). Using LSTAs, all 2^n of these tests can be performed simultaneously. We use trees corresponding to the set of vectors $\{(0, 0, \dots, 1), \dots, (0, 1, \dots, 1), (1, 1, \dots, 1)\}^5$ simultaneously as both the precondition and the postcondition. The corresponding LSTA can be found in Fig. 13, with the number of transitions linear to the number of qubits. We note three key observations: (i) the set of vectors is linearly independent, (ii) the vectors do not represent quantum states, which is fine due to the linearity of quantum gate operations, and (iii) each vector has a unique number of ones; therefore, every vector has a distinct *Euclidean norm*. Since quantum gates are unitary operators, this norm is preserved, ensuring that there will be exactly one vector with the specified norm in the output. Note that not all linearly independent set of vectors can be used, such as the standard basis of \mathbb{R}^{2^n} , since the vectors there have the same norm, so we would lose the one-to-one correspondence between the input and output vectors.

4.4 Verification of Amplitude Constraints

Similarly to the work of [18], LSTAs can be extended to support symbolic amplitudes. For example, when verifying an amplitude amplification algorithm (such as Grover's search [30]), we can use variables v_h and v_l as amplitudes (leaf labels) of the LSTA representing the precondition and describe the relation between the two variables using a global constraint, such as $\varphi: |v_h + 3v_l| > |2v_h|$, which was used in [18] for Grover's search. A tree accepted by such an LSTA is in Fig. 14a and the output obtained after symbolically executing a circuit C that amplifies the amplitude of $|00\rangle$

⁵The set can be defined formally as the set $\{(b_1, b_2, \dots, b_{2^n}) \in \{0, 1\}^{2^n} \mid 0 \leq b_1 \leq b_2 \leq \dots \leq b_{2^n} = 1\}$.

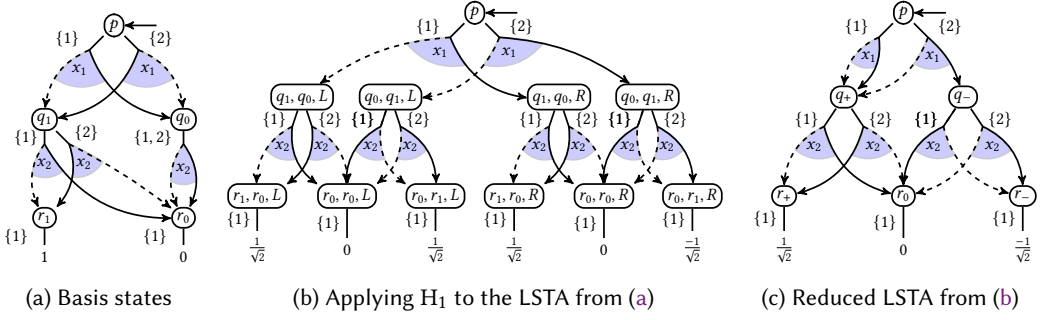


Fig. 15. An example of applying a single-qubit gate on a set of quantum states represented using an LSTA.

over the tree is in Fig. 14b. At the post-condition LSTA, we label the leaves with predicates in the form of $|\square|^2 > |x|^2$ or $|\square|^2 > 90\%$ to denote that the matching leaf probability (denoted as $|\square|^2$) should be bigger than the value of the precondition $|x|^2$ or the constant 90 %, respectively, for x being some of the used variables. In Fig. 14c, we demonstrate an example of a tree accepted by the post-condition LSTA. Notice that if we put all leaf amplitudes of Fig. 14b into the matching \square of the tree in Fig. 14c, the resulting formula is implied by the global constraint ϕ . For example, for the branch $|00\rangle$, we have that $|v_h + 3v_l| > |2v_h| \implies |\frac{v_h + 3v_l}{2}|^2 > |v_h|^2$ is valid. In such a case, we say that the resulting tree is accepted in the post-condition. The symbolic extension would allow us to verify a circuit against properties such as that the full Grover's circuit has $>90\%$ probability of finding a correct answer or that an *amplitude amplification* algorithm increases the probability of finding a correct answer in each iteration.

5 Quantum Gates Operations

Assuming that preconditions and postconditions are given as LSTAs, our next step in the verification of a quantum circuit is to compute the set of states reachable from the precondition after executing the circuit. In this section, we will show, given an LSTA \mathcal{A} representing a set of quantum states and a quantum gate U , how to construct another LSTA $U(\mathcal{A})$ with $\mathcal{L}(U(\mathcal{A})) = \{U(T) \mid T \in \mathcal{L}(\mathcal{A})\}$. Applying the construction for each gate in the circuit, we will then obtain an LSTA representing the set of reachable quantum states.

5.1 General Single-Qubit Gate

Let $\mathcal{A} = \langle Q, \Sigma, \Delta, \mathcal{R} \rangle$ be an LSTA representing a set of quantum states and U be a single-qubit gate $U = \begin{pmatrix} u_1 & u_2 \\ u_3 & u_4 \end{pmatrix}$. Recall that applying U to the t -th qubit of a quantum state combines the 0-subtree T_0 and the 1-subtree T_1 under each node labelled with x_t . For every pair of T_0 and T_1 under a node labeled x_t , with leaf amplitudes of a_1, a_2, \dots, a_k and b_1, b_2, \dots, b_k respectively, the new state will have a new 0-subtree with the amplitudes $(u_1 \cdot a_1 + u_2 \cdot b_1), (u_1 \cdot a_2 + u_2 \cdot b_2), \dots, (u_1 \cdot a_k + u_2 \cdot b_k)$, and a 1-subtree with the amplitudes $(u_3 \cdot a_1 + u_4 \cdot b_1), (u_3 \cdot a_2 + u_4 \cdot b_2), \dots, (u_3 \cdot a_k + u_4 \cdot b_k)$. The construction is lifted from trees to LSTAs in Algorithm 1. The algorithm first constructs the transitions of $U_t(\mathcal{A})$, which are partitioned into the following four sets:

- $\Delta'_{<t}$ indicates that the transitions of qubits before x_t remain the same.
- $\Delta'_{=t}$ initiates a product construction, where both the left-hand side state q_l and the right-hand side state q_r operate simultaneously. The symbols L and R are used to remember the operation to perform when the construction reaches the leaves; L -labeled states combine leaf values using u_1 and u_2 while R -labeled ones use u_3 and u_4 .

Algorithm 1: Application of a single-qubit gate on an LSTA**Input:** An LSTA $\mathcal{A} = \langle Q, \Sigma, \Delta, \mathcal{R} \rangle$ and a gate $U_t = \begin{pmatrix} u_1 & u_2 \\ u_3 & u_4 \end{pmatrix}$ **Output:** $U_t(\mathcal{A})$

- 1 $\Delta'_{<t} := \{q \xrightarrow{-C} x_i(q_l, q_r) \in \Delta \mid i < t\};$
- 2 $\Delta'_{=t} := \{q \xrightarrow{-C} x_t((q_l, q_r, L), (q_l, q_r, R)) \mid q \xrightarrow{-C} x_t(q_l, q_r) \in \Delta\};$
- 3 $\Delta'_{>t} := \{(q_l, q_r, D) \xrightarrow{-C_1 \cap C_2} x_i((q_l^l, q_r^l, D), (q_r^l, q_r^r, D)) \mid i > t \wedge q_l \xrightarrow{-C_1} x_i(q_l^l, q_r^l), q_r \xrightarrow{-C_2} x_i(q_r^l, q_r^r) \in \Delta, D \in \{L, R\}\};$
- 4 $\Delta'_0 := \{(q_l, q_r, L) \xrightarrow{-C_1 \cap C_2} u_1 \cdot a + u_2 \cdot b, (q_l, q_r, R) \xrightarrow{-C_1 \cap C_2} u_3 \cdot a + u_4 \cdot b \mid q_l \xrightarrow{-C_1} a, q_r \xrightarrow{-C_2} b \in \Delta\};$
- 5 $Q' := Q \cup (Q \times Q \times \{L, R\}); \Delta' := \Delta'_{<t} \cup \Delta'_{=t} \cup \Delta'_{>t} \cup \Delta'_0; \Sigma' := \Sigma \cup \{u_1 \cdot a + u_2 \cdot b, u_3 \cdot a + u_4 \cdot b \mid a, b \in \Sigma_0\};$
- 6 **return** $\langle Q', \Sigma', \Delta', \mathcal{R} \rangle;$

- $\Delta'_{<t}$ continues the product construction while remembering L and R and taking the intersection of the choices from both sides.
- Δ'_0 combines the probability amplitude of the leaves based on the symbol L and R .

The H gate is a special case of a single-qubit gate, with $u_1 = u_2 = u_3 = \frac{1}{\sqrt{2}}$, and $u_4 = -\frac{1}{\sqrt{2}}$. An example of applying the H gate to an LSTA can be found in Fig. 15, and the result of applying our LSTA reduction algorithm (Section 6.3) to simplify its structure further can be found in Fig. 15c.

THEOREM 8. $\mathcal{L}(U_t(\mathcal{A})) = \{U_t(T) \mid T \in \mathcal{L}(\mathcal{A})\}$ and $|U_t(\mathcal{A})| = O(|\mathcal{A}|^2)$.

5.2 Controlled Gate

For simplification, we will focus on the controlled gate CU_t^c . This gate applies a single-qubit gate U_t when the control qubit x_c is 1. We will be using the LSTA $\mathcal{A} = \langle Q, \Sigma, \Delta, \mathcal{R} \rangle$ as the input.

While constructing $CU_t^c(\mathcal{A})$, when we encounter a transition labeled with the control qubit x_c , on the 0-subtree, we want to simulate the behavior of \mathcal{A} (because nothing should change when the control qubit is 0), while on the 1-subtree, we want to simulate the LSTA $U_t(\mathcal{A})$. We, however, also need to keep the synchronization between the 0- and 1-subtrees in order not to mix the 0-subtree of one quantum state with the 1-subtree of another quantum state from $\mathcal{L}(\mathcal{A})$.

Our algorithm is built on top of Algorithm 1, which computes the LSTA $U_t(\mathcal{A})$. The main benefit of having $U_t(\mathcal{A})$ is that the x_c -labeled transitions in $U_t(\mathcal{A})$ have the information from both \mathcal{A} and $U_t(\mathcal{A})$ on both 0- and 1- subtrees stored in product states

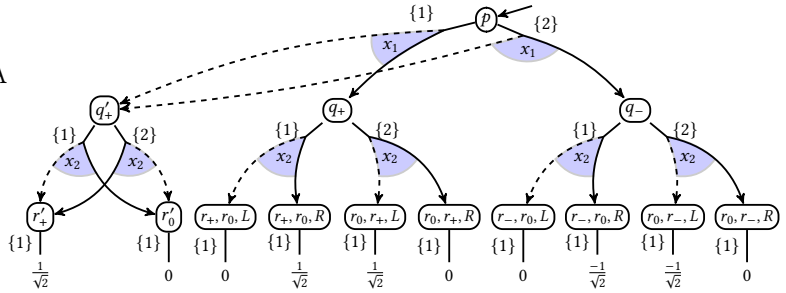


Fig. 16. An LSTA obtained after applying CX_2^1 to the LSTA in Fig. 15c

(states from $Q \times Q \times \{L, R\}$). Therefore, we only need to adjust its 0-subtree to stay in \mathcal{A} .

We present the full construction in Algorithm 2. The algorithm updates transitions from $U_t(\mathcal{A})$ labeled with the control qubit x_c such that the 0-branch will connect to the corresponding state in the transition system of \mathcal{A}' , a primed copy of the input LSTA (Lines 3–6). For the case of $c < t$, we simply redirect the 0-branch from the state q_1 to its primed version q'_1 . When $c > t$, q_1 is a product state of the form (q_a, q_b, D) for $D \in \{L, R\}$, so we reconnect q_1 to q'_a for the L case and to q'_b for the R case. The construction keeps all other transitions intact. We provide an example in Fig. 16. We can generalize it to multi-control gates by allowing more controlled qubits at Line 3.

THEOREM 9. $\mathcal{L}(CU_t^c(\mathcal{A})) = \{CU_t^c(T) \mid T \in \mathcal{L}(\mathcal{A})\}$ and $|CU_t^c(\mathcal{A})| = |\mathcal{A}| + |U_t(\mathcal{A})|$.

Algorithm 2: Application of a controlled gate on an LSTA**Input:** An LSTA $\mathcal{A} = \langle Q, \Sigma, \Delta, \mathcal{R} \rangle$, a single-qubit gate $U_t = \begin{pmatrix} u_1 & u_2 \\ u_3 & u_4 \end{pmatrix}$, a control qubit x_c **Output:** $\text{CU}_t^c(\mathcal{A})$

```

1 Build  $U_t(\mathcal{A}) = \langle Q^U, \Sigma^U, \Delta^U, \mathcal{R} \rangle$  using Algorithm 1, with  $Q^U = Q \cup (Q \times Q \times \{L, R\})$ ;
2 Build  $\mathcal{A}' = \langle Q', \Sigma, \Delta', \mathcal{R}' \rangle$ , a primed copy of  $\mathcal{A}$ ;
3 foreach  $\delta = q \rightarrow x_c(q_1, q_2) \in \Delta^U$  do
4   if  $q_1 \in Q$  then replace  $\delta$  with  $q \rightarrow x_c(q'_1, q_2)$  in  $\Delta^U$ ;           // case  $c < t$ 
5   else if  $q_1 = (q_a, q_b, L)$  then replace  $\delta$  with  $q \rightarrow x_c(q'_a, q_2)$  in  $\Delta^U$ ;
6   else if  $q_1 = (q_a, q_b, R)$  then replace  $\delta$  with  $q \rightarrow x_c(q'_b, q_2)$  in  $\Delta^U$ ;
7 return  $\langle Q^U \cup Q', \Sigma^U \cup \Sigma, \Delta^U \cup \Delta', \mathcal{R} \rangle$ 

```

5.3 Optimizations for the X Gates and Diagonal Matrix Gates

Most single-qubit gates implemented in state-of-the-art quantum computers belong to this category, making it worth considering for special treatment. Note that these constructions are similar to the *permutation-based* construction in [19], but differ in the need for the treatment of choices.

We first show the construction of the LSTA for the X_t gate. For an LSTA \mathcal{A} , we can capture the effect of the X_t gate to all quantum states in $\mathcal{L}(\mathcal{A})$ by swapping the left and the right children of all x_t -labeled transitions $q \rightarrow x_t(q_0, q_1)$, i.e., update them to $q \rightarrow x_t(q_1, q_0)$. All other transitions will stay the same. We use $X_t(\mathcal{A})$ to denote the LSTA constructed following this procedure.

THEOREM 10. $\mathcal{L}(X_t(\mathcal{A})) = \{X_t(T) \mid T \in \mathcal{L}(\mathcal{A})\}$ and $|\mathcal{L}(X_t(\mathcal{A}))| = |\mathcal{A}|$.

Applying the diagonal matrix gate $D_t^{r_0, r_1}$ on the qubit x_t multiplies all leaves of all 0-subtrees rooted in x_t nodes with r_0 and leaves of 1-subtrees rooted therein with r_1 . The construction is formally given in Algorithm 3. In the algorithm, internal x_t -transitions $q \rightarrow x_t(q_0, q_1)$ are modified to $q \rightarrow x_t(q_0, q'_1)$, where q'_1 is a copy of q_1 in the primed version \mathcal{A}' of \mathcal{A} . Then all leaves in \mathcal{A} are multiplied by r_0 and all leaves in \mathcal{A}' are multiplied by r_1 .

THEOREM 11. $\mathcal{L}(D_t^{r_0, r_1}(\mathcal{A})) = \{D_t^{r_0, r_1}(T) \mid T \in \mathcal{L}(\mathcal{A})\}$ and $|\mathcal{L}(D_t^{r_0, r_1}(\mathcal{A}))| = 2|\mathcal{A}|$.

6 LSTA Algorithms

With the algorithms of LSTA quantum gates operations, we can now compute the set of reachable states from the precondition, represented as LSTA. We can then check if all reachable states are allowed by the postcondition, using the language inclusion algorithm we are going to present in this section. Besides language inclusion, we will cover other decision problems, complexity, and algorithms of LSTA in this section for a complete presentation.

Algorithm 3: Application of a diagonal matrix gate on an LSTA**Input:** An LSTA $\mathcal{A} = \langle Q, \Sigma, \Delta, \mathcal{R} \rangle$, a diagonal matrix gate $D_t^{r_0, r_1}$ **Output:** $D_t^{r_0, r_1}(\mathcal{A})$

```

1 Build  $\mathcal{A}' = \langle Q', \Sigma, \Delta', \mathcal{R}' \rangle$ , a primed copy of  $\mathcal{A}$ ;
2 Replace internal  $x_t$ -transitions  $q \rightarrow x_t(q_0, q_1)$  from  $\Delta$  with  $q \rightarrow x_t(q_0, q'_1)$ ;
3 Replace leaf transitions  $q \rightarrow k$  from  $\Delta$  with  $q \rightarrow r_0 \cdot k$ ; Add  $r_0 \cdot k$  to  $\Sigma$ ;
4 Replace leaf transitions  $q' \rightarrow k$  from  $\Delta'$  with  $q' \rightarrow r_1 \cdot k$ ; Add  $r_1 \cdot k$  to  $\Sigma$ ;
5 return  $\langle Q \cup Q', \Sigma, \Delta \cup \Delta', \mathcal{R} \rangle$ ;

```

Algorithm 4: LSTA non-emptiness algorithm**Input:** An LSTA $\mathcal{A} = \langle Q, \Sigma, \Delta, \mathcal{R} \rangle$ with $\mathcal{R} \neq \emptyset$ **Output:** true iff $\mathcal{L}(\mathcal{A}) \neq \emptyset$

```

1 Guess  $r \in \mathcal{R}$  and assign  $S \leftarrow \{r\}$ ;
2 while  $S \neq \emptyset$  do
3   Let  $\Gamma \subseteq \Delta$  be a nondeterministically constructed set of transitions such that for all  $q \in S$ ,
     there is exactly one transition  $\delta_q \in \Gamma$  such that  $\text{top}(\delta_q) = q$ ;
4   if  $\Gamma$  does not exist or  $\bigcap_{\delta \in \Gamma} \ell(\delta) = \emptyset$  then return false;
5    $S := \{q_1, q_2 \mid q \xrightarrow{-C} f(q_1, q_2) \in \Gamma\}$ ;
6 return true;
```

6.1 Intersection, Union, Complementation, and Emptiness Testing

THEOREM 12. *LSTAs are closed under union and intersection but not closed under complementation.*

PROOF. **Complementation** Fix a set of ranked alphabet $\Sigma = \{x, a\}$, we can construct an LSTA accepting empty language, however, we will show in Theorem 17 that we cannot construct one accepting all possible trees using Σ .

Union Let $\mathcal{A}^j = \langle Q^j, \Sigma, \Delta^j, \mathcal{R}^j \rangle$, for $j = 1, 2$, be two LSTAs, their union $\mathcal{A}_1 \cup \mathcal{A}_2$ can be constructed by combining the transition systems of \mathcal{A}_1 and \mathcal{A}_2 . This involves creating a disjoint union of their states, transitions, root states, and symbols. That is,

$$\mathcal{A}_{1 \cup 2} = \langle Q, \Sigma, \Delta, \mathcal{R} \rangle, \text{ where } Q = Q^1 \uplus Q^2, \mathcal{R} = \mathcal{R}^1 \uplus \mathcal{R}^2, \text{ and } \Delta = \Delta^1 \uplus \Delta^2.$$

Intersection On the other hand, their intersection can be constructed via a *product construction* and reassign each pair of choices to a fresh number. That is,

$$\mathcal{A}_{1 \cap 2} = \langle Q', \Sigma, \Delta', \mathcal{R}' \rangle, \text{ where } Q' = Q^1 \times Q^2, \mathcal{R}' = \mathcal{R}^1 \times \mathcal{R}^2, \text{ and}$$

$$\Delta' = \{(q^1, q^2) \xrightarrow{-N(C^1 \times C^2)} f((q_l^1, q_l^2), (q_r^1, q_r^2)) \mid q^1 \xrightarrow{-C^1} f(q_l^1, q_r^1) \in \Delta^1 \wedge q^2 \xrightarrow{-C^2} f(q_l^2, q_r^2) \in \Delta^2\} \\ \cup \{(q^1, q^2) \xrightarrow{-N(C^1 \times C^2)} k \mid q^1 \xrightarrow{-C^1} k \in \Delta^1 \wedge q^2 \xrightarrow{-C^2} k \in \Delta^2\}$$

Here, $N(C^1 \times C^2)$ is a set of choices obtained by mapping every choice pair in $C^1 \times C^2$ to a unique number in \mathbb{N} . Proofs of the correctness of these constructions are standard. \square

THEOREM 13. *LSTA emptiness is **PSPACE**-complete.*

PROOF. **PSPACE-membership** We will show that LSTA non-emptiness is in **NPSPACE**, which implies that LSTA emptiness is in **co-NPSPACE**, and the result will follow by the Immerman–Szelepcsényi theorem (**co-NPSPACE** = **NPSPACE**) and Savitch’s theorem (**NPSPACE** = **PSPACE**).

By Algorithm 4, we show that LSTA non-emptiness is in **NPSPACE**. At every step, Algorithm 4 only remembers the current value of S , Γ , and the new values of S , which are all of a polynomial size w.r.t. the size of \mathcal{A} . The algorithm takes advantage of the fact that at every level of a LSTA run, the transitions should take the same choice, and therefore all occurrences of q at a level must agree on the same transition. As a result, the subtrees of the same state q at a level are also the same, and, therefore, we need to keep track of only one occurrence.

PSPACE-hardness By reduction from the **PSPACE**-complete problem of universality of a *non-deterministic finite automaton* (NFA) that has in each state over every symbol exactly two non-deterministic transitions. One can show that universality for this sub-class of NFAs is still **PSPACE**-hard, e.g., by modifying the standard proof in [25, Theorem 3.13]. The proof in [25] goes by

reduction from the **PSPACE**-complete problem of membership of a string in the language of a linearly bounded automaton (LBA). It constructs an NFA that rejects a sequence of configurations that corresponds to an accepting run of the LBA, and accepts all other sequences of symbols. So it holds that the input is not in the language of the LBA iff the language of the NFA is universal. This can be modified for the considered class of NFAs by relaxing the structure of the LBA's configurations, allowing to use “empty symbols” on the tape. Details are technical.

Let $\mathcal{M} = (Q, \Sigma, \delta, I, F)$ be an NFA of the class above over (standard unranked) alphabet Σ with the sets of initial and final states $I, F \subseteq Q$ and the transition function $\delta: Q \times \Sigma \rightarrow 2^Q$, where it holds for all $q \in Q$ and $a \in \Sigma$ that $|\delta(q, a)| = 2$ as mentioned above. W.l.o.g., we assume that \mathcal{M} contains at least one initial state and that $\Sigma = \{1, \dots, n\}$. We construct the LSTA $\mathcal{A}_{\mathcal{M}} = (Q, \{\clubsuit, \circ\}, \Delta_{\delta}, I)$ where \clubsuit and \circ are new symbols with arity 0 and 2 respectively. The LSTA, intuitively, works as follows: Symbols from $\Sigma \cup \{0\}$ are encoded into choices on transitions. The tree generated by $\mathcal{A}_{\mathcal{M}}$ corresponds to the computational tree of the textbook algorithm performing universality check on \mathcal{M} by doing on-the-fly determinization and checking for a macrostate that contains no state from F . $\mathcal{A}_{\mathcal{M}}$ will accept such a tree because only states that are non-accepting in \mathcal{M} contain a leaf transition in $\mathcal{A}_{\mathcal{M}}$ (synchronized using choice 0). Formally, Δ_{δ} is defined as follows:

$$\Delta_{\delta} = \{q \dashv 0 \mapsto \clubsuit \mid q \notin F\} \cup \{q \dashv i \mapsto \circ(q_1, q_2) \mid \delta(q, i) = \{q_1, q_2\}\}, \quad (1)$$

It holds that the (word) language of \mathcal{M} is not Σ^* iff the (tree) language of $\mathcal{A}_{\mathcal{M}}$ is non-empty. \square

6.2 Entailment Testing

THEOREM 14. *The inclusion of languages of two LSTAs is decidable.*

PROOF. Reduce to graph reachability The inclusion $\mathcal{L}(\mathcal{A}) \subseteq \mathcal{L}(\mathcal{B})$ between two LSTAs $\mathcal{A} = \langle Q_{\mathcal{A}}, \Sigma, \Delta_{\mathcal{A}}, \mathcal{R}_{\mathcal{A}} \rangle$ and $\mathcal{B} = \langle Q_{\mathcal{B}}, \Sigma, \Delta_{\mathcal{B}}, \mathcal{R}_{\mathcal{B}} \rangle$ can be reduced to graph reachability in a directed graph (V, A) , with the vertices in V of the form $(D, \{F_1, \dots, F_m\})$ where $D \subseteq Q_{\mathcal{A}}$ is the *domain* and $F_i: D \rightarrow 2^{Q_{\mathcal{B}}}$ is a total map that assigns sets of states of \mathcal{B} to states of \mathcal{A} from the domain D . The algorithm makes use of the following essential property of trees generated by an LSTA \mathcal{A} : if two nodes at the same level of a tree T are labelled by the same state in an accepting run of \mathcal{A} on T , then the subtrees rooted in these nodes are identical (this follows from the semantics of LSTAs and the restriction on transitions, cf. Section 3.1).

Intuitively, D represents the set of states of \mathcal{A} in a level of a run ρ of \mathcal{A} , and every F_i represents the same level of some possible run ρ_i of \mathcal{B} on the same tree, and how it can cover the run ρ of \mathcal{A} . For instance, in Fig. 17, the state q of \mathcal{A} corresponds to the states r and s of \mathcal{B} because they are used in the same tree level and the same tree nodes. So we have $F_i(q) = \{r, s\}$. Due to the property that all occurrences of a state at the same level in a run generate the same subtree mentioned above, we only need to maintain encountered states and their alignment with each other.

Source and terminal vertices They correspond to the root and leaf tree levels, respectively.

- (1) A vertex $(\{q\}, \{\{q \mapsto r_1\}, \dots, \{q \mapsto r_k\}\})$ with $q \in \mathcal{R}_{\mathcal{A}}$ and $\mathcal{R}_{\mathcal{B}} = \{r_1, \dots, r_k\}$ is a *source* vertex. Intuitively, both automata start their runs in their root states.

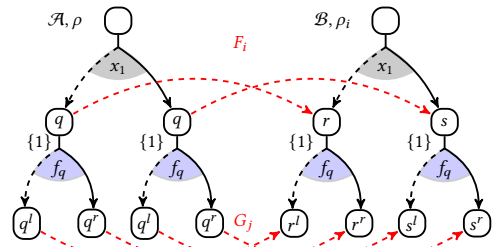


Fig. 17. Computing G_j from F_i

- (2) A vertex (\emptyset, \mathcal{F}) where $\emptyset \notin \mathcal{F}$ is a *terminal* vertex. Intuitively, empty domain means that at that level of the run of \mathcal{A} , all branches of the tree have already ended at leaves, hence \mathcal{A} accepts the tree. On the other hand, $\emptyset \notin \mathcal{F}$ means that \mathcal{B} did not have any run on the same tree that would end at leaves and accept. The tree is therefore accepted only by \mathcal{A} .

Arrows Starting from a vertex $U = (D, \{F_1, \dots, F_m\})$, we construct an arrow (U, V) with $V = (E, \mathcal{G})$ as follows. First, we construct sets of transitions outgoing from D such that in each set $\Gamma_{\mathcal{A}}$, we select exactly one downward transition $\delta_{q_{\mathcal{A}}}$ originating from each $q_{\mathcal{A}} \in D$, such that all transitions in $\Gamma_{\mathcal{A}}$ share a common choice (as required by the definition of an accepting run (cf. Section 3.1)). Formally, given $D = \{q_1, \dots, q_k\}$, we consider all sets of transitions $\Gamma_{\mathcal{A}} = \{\delta_1, \dots, \delta_k\}$ such that the following formula holds:

$$(\forall 1 \leq i \leq k: \delta_i \in \Delta \wedge \text{top}(\delta_i) = q_i) \quad \wedge \quad \bigcap \{\ell(\delta_i) \mid 1 \leq i \leq k\} \neq \emptyset. \quad (2)$$

The domain of the target V is then obtained from $\Gamma_{\mathcal{A}}$ as the set $E = \{q^l, q^r \mid q \text{--} C \rightarrow f_q(q^l, q^r) \in \Gamma_{\mathcal{A}}\}$. If all transitions in $\Gamma_{\mathcal{A}}$ are leaf transitions, then $E = \emptyset$. We note that it is perfectly possible that no $\Gamma_{\mathcal{A}}$ exists for some vertex U , in which case U has no successor.

For the construction of \mathcal{G} , we need to maintain the correspondences recorded in F_1, \dots, F_m . Therefore, for every set $\Gamma_{\mathcal{A}}$ and every mapping $F_i \in \mathcal{F}$, we create a set of mappings $\{G_1, \dots, G_n\}$ as follows: First, we construct sets $\Gamma_{\mathcal{B}}$ of (synchronized) transitions leaving $\text{img}(F_i)$ in the same way as in Eq. (2) (with D substituted by $\text{img}(F_i)$). Then, for every transition $\delta_{\mathcal{A}} \in \Gamma_{\mathcal{A}}$, we find the corresponding transition $\delta_{\mathcal{B}}$ in the current $\Gamma_{\mathcal{B}}$ (i.e., such that $\text{top}(\delta_{\mathcal{B}}) \in F_i(\text{top}(\delta_{\mathcal{A}}))$). For the pair $\delta_{\mathcal{A}}$ and $\delta_{\mathcal{B}}$, we then check whether their symbols match, and if not, we dismiss the pair $\Gamma_{\mathcal{A}}$ and $\Gamma_{\mathcal{B}}$. On the other hand, if the symbols of all such pairs of transitions match, we construct the new state mapping G_j such that for every $q \in E$, we set

$$G_j(q) = \left\{ s_q^l \mid p \text{--} C \rightarrow f(q, q^r) \in \Gamma_{\mathcal{A}}, s \in F_i(p), s \text{--} C' \rightarrow f(s_q^l, s_q^r) \in \Gamma_{\mathcal{B}} \right\} \cup \left\{ s_q^r \mid p \text{--} C \rightarrow f(q^l, q) \in \Gamma_{\mathcal{A}}, s \in F_i(p), s \text{--} C' \rightarrow f(s_q^l, s_q^r) \in \Gamma_{\mathcal{B}} \right\}.$$

We then merge all sets $\{G_1, \dots, G_n\}$ for all F_i 's into one set \mathcal{G} and construct the vertex (E, \mathcal{G}) .

The graph is finite because $Q_{\mathcal{A}}$ and $Q_{\mathcal{B}}$ are finite. The inclusion holds iff the graph has no path from a source to a terminal vertex.

Witness of $\mathcal{L}(\mathcal{A}) \not\subseteq \mathcal{L}(\mathcal{B})$ If we also remember the set $\Gamma_{\mathcal{A}}$ in the graph vertex, we can construct the tree to witness the non-inclusion following the path from a source vertex to a terminal vertex. Recall that the D part of a vertex $(D, \{F_1, \dots, F_m\})$ corresponds to a tree level of \mathcal{A} , and the set $\Gamma_{\mathcal{A}}$ gives the information on how the levels are linked together to form a tree.

THEOREM 15. *The LSTA language inclusion problem is **PSPACE**-hard and in **EXSPACE**.*

PROOF. We can show that the problem is **PSPACE**-hard by a trivial reduction from the emptiness problem (Theorem 13). For the upper bound, let us analyze the complexity of the inclusion algorithm from the proof of Theorem 14. How many vertices are there in the graph? Since every node of the graph has the structure $(D, \{F_1, \dots, F_m\})$, the set of vertices is included in the set $2^{Q_{\mathcal{A}}} \times 2^{Q_{\mathcal{A}} \rightarrow 2^{Q_{\mathcal{B}}}} = 2^{Q_{\mathcal{A}}} \times 2^{((2^{Q_{\mathcal{B}}})^{Q_{\mathcal{A}}})}$ (we can change the original definition of F_i to be a mapping of the type $F_i: Q_{\mathcal{A}} \rightarrow 2^{Q_{\mathcal{B}}}$). We can then bound the number of vertices by the number

$$2^{|Q_{\mathcal{A}}|} \cdot 2^{((2^{Q_{\mathcal{B}}})^{|Q_{\mathcal{A}}|})} = 2^{|Q_{\mathcal{A}}|} \cdot 2^{(2^{Q_{\mathcal{B}}| \cdot |Q_{\mathcal{A}}|})} = 2^{|Q_{\mathcal{A}}| + (2^{Q_{\mathcal{B}}| \cdot |Q_{\mathcal{A}}|})} \quad (3)$$

The size of one node is then in $\mathcal{O}(|Q_{\mathcal{A}}| + (2^{Q_{\mathcal{B}}| \cdot |Q_{\mathcal{A}}|}))$, i.e., exponential. Since inclusion is checked by graph reachability, we can conclude that the problem is in **EXSPACE**. \square

Algorithm 5: LSTA reduction

Input: An LSTA $\mathcal{A} = \langle Q, \Sigma, \Delta, \mathcal{R} \rangle$
Output: A reduced LSTA with the same language as \mathcal{A}

```

1 changed := true;
2 while changed do
3   changed := false;
4   foreach  $\delta_1 = q \rightarrow x(B)$  and  $\delta_2 = q \rightarrow x(B) \in \Delta$  s.t.  $C_1 \neq C_2$  and  $B \in Q^0 \cup Q^2$  do
5      $\Delta := (\Delta \setminus \{\delta_1, \delta_2\}) \cup \{q \rightarrow x(B)\}$ ; changed := true;
6   foreach  $p, q \in Q$  s.t.  $p \neq q$  do
7     if  $\forall B \in Q^0 \cup Q^2, C \subseteq \mathbb{N}_0, x \in \Sigma: q \rightarrow x(B) \in \Delta \Leftrightarrow p \rightarrow x(B) \in \Delta$  then
8       Merge  $p$  and  $q$ ; changed := true;
9 return  $\mathcal{A}$ ;
```

6.3 LSTA Reduction

After executing corresponding operations for gates in the circuit on the precondition LSTA, the size of the LSTA may increase exponentially w.r.t. the number of gates, even though each gate operation is bounded by a quadratic factor. In practice, we employ a simple reduction algorithm for LSTAs (Algorithm 5), which significantly aids in controlling the size of the generated LSTAs. The algorithm effectively performs reduction w.r.t. the bottom-up bisimulation [3], i.e., it merges two states with the same downward-behavior (Lines 6–8). In addition, the algorithm also deals with transitions that are the same except for the set of choices—such transitions can be merged into one (Lines 4–5). An example of the output of a reduction can be found in Fig. 15c. When run on LSTAs that are acyclic (e.g., they represent quantum states with a fixed number of qubits), the algorithm can be optimized by considering states in an order starting from states that only have leaf symbols, going upwards, level by level.

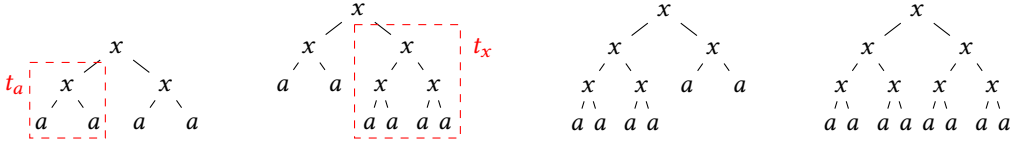
6.4 Comparison with the Traditional Tree Automata Model

In traditional top-down deterministic tree automata (TAs), we would require the set of possible transitions leaving q under f to be of cardinality one. With LSTAs, we allow this set to be larger, but at every level of the run, the transitions should take the same choice. In contrast, a traditional TA is almost the same with LSTA, with the exception that it does not use the labeled choices for synchronization. Other modifications of traditional tree automata that allow global constraints to go beyond regularity has been considered in the literature [13, 27, 32, 33, 47]. However, none of them permits language inclusion test, which is essential for symbolic verification.

THEOREM 16 (SUCCINCTNESS). *Traditional TAs need at least 2^{n-1} transitions to encode all n -qubits GHZ states.*

PROOF. If we view each GHZ state as a tree (Fig. 5), there are 2^{n-1} 0-subtrees, and each 1-subtree corresponds to a unique 0-subtree. Using traditional tree automata without synchronization, we would require 2^{n-1} root transitions, each connecting to a unique pair of one 0-subtree and two 1-subtrees. If there were fewer root transitions, then there would be two different 0-subtrees generated by the same root transition, and any generated 1-subtree could be paired with both of them. This contradicts the condition that each 1-subtree corresponds to a unique 0-subtree. \square

General quantum gates create a correspondence between the subtrees (cf. Section 2.2.1 and Fig. 7), and, hence, level-synchronization is critical in representing such sets of quantum states concisely.

Fig. 19. Trees of $n = 1$ have 2^2 varieties as branches below level 1

THEOREM 17. *The class of languages recognized by LSTAs is incomparable to regular tree languages.*

PROOF. Intuitively, we show that (i) LSTAs can accept sets of all perfect trees of an arbitrary height using their synchronization mechanism (while traditional TAs cannot) and, on the other hand, (ii) LSTAs cannot accept the set of all trees (with each branch having an arbitrary length), while traditional TAs can.

TA $\not\subseteq$ LSTA Here we define an LSTA $\mathcal{A} = \langle \{p, q\}, \{x, a\}, \Delta, \{p\} \rangle$ accepting all perfect binary trees whose leaves are labeled a and internal nodes are labeled x . The LSTA is defined in Fig. 18. We use the choices to force trees to make a consistent decision at each tree level: either all transitions generate leaves (choice 2) or internal nodes (choice 1). We will show that the language of this LSTA is not expressible by traditional TAs. We assume that there is a traditional TA \mathcal{A} accepting all such states, which is an infinite set of perfect trees. We use q_l^i and q_r^i to denote the left and right bottom states, respectively, of the root transition of some of \mathcal{A} 's accepting run on a tree with height i . Since there are a finite number of states in \mathcal{A} , and there are infinitely many accepted trees of different heights, there must be two different heights, i and j , such that $q_l^i = q_l^j$. This leads us to the conclusion that q_l^i has (due to non-determinism) at least two possible subtrees with different heights below it. Since there is no synchronizing mechanism between states at the same level, q_l^i can choose a subtree whose height is different from the height of q_r^i 's subtree. Therefore, \mathcal{A} can accept a tree that is not perfect and, therefore, does not encode the set of perfect trees.

LSTA $\not\subseteq$ TA For the other direction, consider the non-deterministic traditional TA $\mathcal{A} = \langle Q = \{q, q_a\}, \Sigma = \{x, a\}, \Delta, \mathcal{R} = \{q\} \rangle$ with transitions $q \rightarrow x(q, q)$, $q \rightarrow x(q_a, q_a)$, $q_a \rightarrow a$. Suppose that $\mathcal{L}(\mathcal{A})$ can be recognized by a LSTA $\mathcal{B} = \langle Q_{\mathcal{B}}, \Sigma, \Delta_{\mathcal{B}}, \mathcal{R}_{\mathcal{B}} \rangle$ with $|Q_{\mathcal{B}}| = m$ states. Let $n \gg 2m$. Consider the trees T that are perfect above height n , with all nodes with height $\leq n$ labeled with x . Their subtrees below height n are either of the form $t_x := x(x(a, a), x(a, a))$ or $t_a := x(a, a)$ (see for instance Fig. 19 for $n = 1$). At height n , there are 2^n tree nodes, and each can pick either subtree t_a or t_x . Hence, there are 2^{2^n} such trees and these trees belong to $\mathcal{L}(\mathcal{A})$. By assumption, there are accepting runs of the LSTA \mathcal{B} associated to these trees. Since each state of \mathcal{B} at the top of a level of a tree run can only choose one unique transition, it follows that at the top of level n , \mathcal{B} must have at least 2 states, say q_x and q_a , in order to cover possible subtrees t_x and t_a respectively. Moreover, q_x and q_a can appear as left or right children of a transition used from level $n - 1$ to level n and there are 2^2 possible pairs as bottoms of transitions. Thus, in order to cover all such trees, it requires at least 2^2 states at the top of level $n - 1$. In a similar fashion we can conclude that it requires at least 2^{2^m} states for level $n - m$ to cover all the tree runs for such trees. However, $2^{2^m} > m$ and it leads to a contradiction to the assumption that $|Q_{\mathcal{B}}| = m$. Thus, the theorem follows. \square

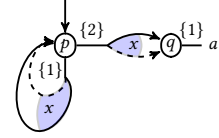


Fig. 18. LSTA recognizing a non-regular tree language

7 Experimental Evaluation

We implemented our LSTA-based verification framework as an updated version of AUTOQ⁶. It is written in C++ and combines the three needed components: the LSTA symbolic representation

⁶<https://github.com/fmlab-iis/AutoQ>

Table 1. Results of experiments. The columns **#q** and **#G** give the number of qubits and gates respectively of the circuit. For **AUTOQ**, we give the times needed to obtain the LSTA representing all outputs of the circuit (post_C), test the inclusion with the post-condition (\subseteq), and the sum of these times (total). The timeout was 5 min. We use colours to distinguish the **best result** and **timeout/out-of-memory**. “—” denotes that the tool was not applicable due to some limitation. The missing blocks for **FLIPGATE** are because the circuits did not contain CX gates. **symQV** timed out on all benchmarks from **CORRECT** and **FLIPGATE** and **CAAL** timed out on all benchmarks in **CORRECT** so we do not show their columns for those cases.

	CORRECT										MissGATE							FlipGATE						
	#q	#G	AutoQ			AutoQ-OLD	SLIQSIM	SV-SIM	AutoQ			AutoQ-OLD	SYMQV	CAAL	AutoQ			AutoQ-OLD	CAAL					
			postC	⊆	total				postC	⊆	total				postC	⊆	total							
BV-Sing	96	241	0.2s	0.0s	0.2s	4.3s	0.0s	OOM	0.2s	0.0s	0.2s	4.8s	TO	TO	0.2s	0.0s	0.2s	4.4s	TO					
	97	243	0.2s	0.0s	0.2s	4.6s	0.0s	OOM	0.2s	0.0s	0.2s	4.8s	TO	TO	0.2s	0.0s	0.2s	4.6s	TO					
	98	246	0.3s	0.0s	0.3s	4.7s	0.0s	OOM	0.2s	0.0s	0.2s	5s	TO	TO	0.3s	0.0s	0.3s	4.7s	TO					
	99	248	0.2s	0.0s	0.2s	4.9s	0.0s	OOM	0.3s	0.0s	0.3s	5.1s	TO	TO	0.3s	0.0s	0.3s	4.8s	TO					
	100	251	0.3s	0.0s	0.3s	5s	0.0s	OOM	0.2s	0.0s	0.2s	5.2s	TO	TO	0.2s	0.0s	0.2s	5s	TO					
BV-All	19	30	0.0s	0.0s	0.0s	2.8s	TO	TO	0.0s	0.0s	0.0s	2.9s	TO	TO	0.0s	0.0s	0.0s	2.9s	TO					
	21	33	0.0s	0.0s	0.0s	8s	TO	TO	0.0s	0.0s	0.0s	7.3s	TO	TO	0.0s	0.0s	0.0s	7.3s	TO					
	23	36	0.0s	0.0s	0.0s	23s	TO	TO	0.0s	0.0s	0.0s	44s	TO	TO	0.0s	0.0s	0.0s	44s	TO					
	25	39	0.0s	0.0s	0.0s	1m11s	TO	TO	0.0s	0.0s	0.0s	1m58s	TO	TO	0.0s	0.0s	0.0s	1m58s	TO					
	27	42	0.0s	0.0s	0.0s	4m45s	TO	TO	0.0s	0.0s	0.0s	TO	TO	TO	0.0s	0.0s	0.0s	TO	TO					
GHZ-Sing	64	64	0.0s	0.0s	0.0s	0.3s	0.0s	OOM	0.0s	0.0s	0.0s	0.4s	TO	TO	0.0s	0.0s	0.0s	0.3s	TO					
	128	128	0.1s	0.0s	0.1s	2.5s	0.0s	OOM	0.1s	0.0s	0.1s	2.5s	TO	TO	0.1s	0.0s	0.1s	2.7s	TO					
	256	256	0.8s	0.0s	0.8s	20s	0.0s	OOM	0.8s	0.0s	0.8s	20s	TO	TO	0.7s	0.0s	0.7s	20s	TO					
	384	384	1.9s	0.0s	1.9s	1m10s	0.1s	OOM	1.9s	0.0s	1.9s	1m12s	TO	TO	1.7s	0.0s	1.7s	1m9s	TO					
	512	512	3.6s	0.0s	3.6s	2m49s	0.1s	OOM	3.6s	0.0s	3.6s	2m59s	TO	TO	3.3s	0.0s	3.3s	2m52s	TO					
GHZ-All	8	8	0.0s	0.0s	0.0s	0.1s	1.5s	0.0s	0.0s	0.0s	0.2s	TO	30s	0.0s	0.0s	0.0s	0.1s	32s						
	16	16	0.0s	0.0s	0.0s	TO	TO	1m37s	0.0s	0.0s	0.0s	TO	TO	TO	0.0s	0.0s	0.0s	TO	55s					
	32	32	0.0s	0.0s	0.0s	TO	TO	OOM	0.0s	0.0s	0.0s	TO	TO	1m28s	0.0s	0.0s	0.0s	TO	1m27s					
	64	64	0.1s	0.0s	0.1s	TO	TO	OOM	0.1s	0.0s	0.1s	TO	TO	TO	0.1s	0.0s	0.1s	TO	3m7s					
	128	128	0.6s	0.0s	0.6s	TO	TO	OOM	0.5s	0.0s	0.5s	TO	TO	TO	0.6s	0.0s	0.6s	TO	TO					
Grover-Sing	24	5215	1.3s	0.0s	1.3s	10s	TO	TO	1.3s	0.0s	1.3s	10s	TO	—	1.5s	0.0s	1.5s	11s	—					
	28	12217	3.8s	0.0s	3.8s	32s	TO	TO	3.9s	0.0s	3.9s	32s	TO	—	4.1s	0.0s	4.1s	35s	—					
	32	28159	10s	0.0s	10s	1m28s	TO	OOM	16s	0.0s	16s	2m35s	TO	—	11s	0.0s	11s	1m41s	—					
	36	63537	26s	0.0s	26s	4m3s	TO	OOM	45s	0.0s	45s	TO	TO	—	28s	0.0s	28s	4m36s	—					
	40	141527	1m8s	0.0s	1m8s	TO	TO	OOM	1m28s	0.0s	1m28s	TO	TO	—	1m13s	0.0s	1m13s	TO	—					
Grover-All	18	357	0.2s	0.0s	0.2s	3.1s	TO	38s	0.2s	0.0s	0.2s	3.6s	TO	TO	0.5s	0.0s	0.5s	10s	TO					
	21	552	0.8s	0.0s	0.8s	10s	TO	TO	0.9s	0.0s	0.9s	12s	TO	—	1.8s	0.0s	1.8s	31s	—					
	24	999	3.0s	0.1s	3.1s	38.1s	TO	TO	3.0s	0.1s	3.1s	44s	TO	—	7.1s	0.2s	7.3s	TO	—					
	27	1492	9.7s	0.8s	10.5s	2m20s	TO	TO	9.8s	0.7s	10.5s	3m38s	TO	—	25s	1.1s	26.1s	TO	—					
	30	2433	36s	3.3s	39.3s	TO	TO	OOM	36s	3.2s	39.2s	TO	TO	—	1m28s	4.2s	1m32s	TO	—					
H2	12	24	0.0s	0.0s	0.0s	40s	1m51s	0.5s	0.0s	0.0s	0.0s	39s	TO	TO	0.0s	0.0s	0.0s	TO	TO					
	13	26	0.0s	0.0s	0.0s	2m35s	TO	TO	2.1s	0.0s	0.0s	2m15s	TO	OOM	0.0s	0.0s	0.0s	TO	TO					
	64	128	0.2s	0.0s	0.2s	TO	TO	OOM	0.2s	0.0s	0.2s	TO	TO	TO	0.2s	0.0s	0.2s	TO	TO					
	128	256	0.9s	0.0s	0.9s	TO	TO	OOM	1.0s	0.0s	1s	TO	TO	TO	1.0s	0.0s	1s	TO	TO					
	256	512	4.4s	0.0s	4.4s	TO	TO	OOM	4.9s	0.0s	4.9s	TO	TO	TO	4.9s	0.0s	4.9s	TO	TO					
HXH	10	30	0.0s	0.0s	0.0s	1.8s	11s	0.0s	0.0s	0.0s	1.1s	TO	TO	0.0s	0.0s	0.0s	TO	TO						
	11	33	0.0s	0.0s	0.0s	4.3s	34s	0.2s	0.0s	0.0s	5.3s	TO	TO	0.0s	0.0s	0.0s	TO	TO						
	12	36	0.0s	0.0s	0.0s	11.1s	1m51s	0.7s	0.0s	0.0s	15s	TO	TO	0.0s	0.0s	0.0s	TO	TO						
	13	39	0.0s	0.0s	0.0s	36.3s	TO	2.9s	0.0s	0.0s	1m51s	TO	TO	0.0s	0.0s	0.0s	TO	TO						
	99	297	0.7s	0.0s	0.7s	TO	TO	OOM	0.7s	0.0s	0.7s	TO	TO	TO	0.7s	0.0s	0.7s	TO	TO					
MCTFOLI	16	15	0s/0s	0s/0s	0.0s/0.0s	0.0s/0.0s	TO	7.7s	0s/0s	0s/0s	0.0s/0.0s	0.0s/0.0s	TO	TO	0s/0s	0s/0s	0.0s/0.0s	0.0s/0.0s	TO					
	20	19	0s/0s	0s/0s	0.0s/0.0s	0.0s/0.0s	TO	TO	0s/0s	0s/0s	0.0s/0.0s	0.0s/0.0s	TO	TO	0s/0s	0s/0s	0.0s/0.0s	0.0s/0.0s	TO					
	24	23	0s/0s	0s/0s	0.0s/0.0s	0.0s/0.0s	TO	TO	0s/0s	0s/0s	0.0s/0.0s	0.0s/0.0s	TO	TO	0s/0s	0s/0s	0.0s/0.0s	0.0s/0.0s	TO					
	28	27	0s/0s	0s/0s	0.0s/0.0s	0.1s/0.1s	TO	TO	0s/0s	0s/0s	0.0s/0.0s	0.1s/0.1s	TO	TO	0s/0s	0s/0s	0.0s/0.0s	0.1s/0.1s	TO					
	32	31	0s/0s	0s/0s	0.0s/0.0s	0.1s/0.2s	TO	OOM	0s/0s	0s/0s	0.0s/0.0s	0.1s/0.1s	TO	TO	0s/0s	0s/0s	0.0s/0.0s	0.2s/0.2s	TO					
Grover-Iter	3	13	0.0s	0.0s	0.0s	0.3s	—	—	0.0s	0.1s	0.1s	TO	4m7s	—	0.0s	0.0s	0.0s	TO	TO					
	36	157	0.0s	0.0s	0.0s	2.0s	—	—	0.0s	0.0s	0.0s	2.3s	TO	—	0.0s	0.0s	0.0s	TO	TO					
	100	445	2.2s	0.0s	2.2s	49s	—	—	2.4s	0.1s	2.5s	55s	TO	—	2.4s	0.1s	2.5s	TO	TO					
	150	671	7.4s	0.1s	7.5s	3m35s	—	—	7.7s	0.1s	7.8s	TO	TO	—	7.7s	0.1s	7.8s	TO	TO					
	200	895	17s	0.1s	17.1s	TO	—	—	18s	0.1s	18.1s	TO	TO	—	18s	0.1s	18.1s	TO	TO					

from Sections 3 and 4, the gate operations from Section 5, and the entailment checking algorithm from Section 6. As an input, **AUTOQ** takes a quantum circuit C in the **OPENQASM** format, a pre-condition LSTA P , and a post-condition LSTA Q . Starting from the pre-condition LSTA P , **AUTOQ** reads the quantum gates from C one by one and executes them symbolically to obtain an output LSTA R . **AUTOQ** then checks if $\mathcal{L}(R) \subseteq \mathcal{L}(Q)$ using the entailment testing algorithm from Section 6. When the test fails, **AUTOQ** reports a reachable quantum state violating the post-condition for diagnostics. We use a precise complex number representation similar to those in [19, 50, 62], with an extension to allow a wider range of angles. For rotation gates such as $R_X(\theta)$ and $R_Z(\theta)$, we allow θ in the form of $\frac{n}{4}\pi$ for $n \in \mathbb{Z}$.

Tools. We compared the new AUTOQ with several state-of-the-art tools. Among these, the only tool directly comparable (as it also performs automated Hoare-style verification) to AUTOQ is its predecessor [18, 19], which uses an approach based on traditional tree automata. Second, we compared AUTOQ against two symbolic quantum circuit verification tools: SYMQV [9], which is based on the SMT theory of reals, and CAAL [20], which is based on an extended SMT theory of arrays. In our evaluation, we specified equivalent functional correctness properties for each benchmark example in their respective specification languages. Third, when the precondition involves a finite number of quantum states, we can solve the verification task by using *quantum circuit simulators* to simulate all allowed initial quantum states and validate against the postcondition. Therefore, we also compared AUTOQ with the state vector-based simulator SV-SIM [37] and the decision diagram-based simulator SLIQSIM [50]. Validation against postcondition is, however, hard for these two simulators because printing the final state as an explicit vector takes too much time. Therefore, we report the time required for circuit simulation and omit the time for validation against the postcondition. This gives us a conservative under-approximation of the time the simulators would need for verification.

Benchmarks. We compared all tools on the following set of benchmarks:

- **BV-SING and BV-ALL:** Bernstein-Vazirani’s algorithm [10] (Section 4.1) with one hidden string and with all possible hidden strings of length n , respectively. For BV-SING, the hidden string is in the form of $|1010 \dots\rangle$; for BV-ALL, hidden strings are decided by input.
- **GHZ-SING and GHZ-ALL:** The GHZ circuit [29] with the pure zero input state $|0^n\rangle$ and with all possible input states $\{|s_1 0 s_2 0 \dots s_n 01\rangle \mid s_1, s_2, \dots s_n \in \mathbb{B}\}$.
- **GROVER-SING and GROVER-ALL:** Grover’s search [30] circuit for a single oracle and for all possible oracles of length n . For the former, the hidden item is $|0101 \dots\rangle$. We verify that the output amplitudes match the expected values.
- **GROVER-ITER:** Verification of one iteration of Grover’s search w.r.t. the symbolic property that the amplitude of the secret is amplified (Section 4.4).
- **H2 and HXH:** the former has two consecutive H gates for each qubit in an n -qubit quantum circuit and the latter has one additional X gate in between the two H gates. Both use all possible computational basis states as the pre-condition.
- **MCTOFFOLI:** circuits implementing multi-control Toffoli gates of size n using a variation of Nielsen and Chuang’s decomposition [44] with standard Toffoli gates. The pre- and post-conditions are those from Section 4.2. We always give a pair of results: for $k=0/k=1$.

We further consider the following three scenarios:

- **CORRECT:** verification of a correct circuit.
- **MISSGATE:** finding a bug in a circuit obtained from a correct one by removing a random gate.
- **FLIPGATE:** finding a bug in a circuit obtained from a correct circuit by selecting a random CX gate and swapping its control and target qubits.

Evaluation and results. We conducted all our experiments on a server running Ubuntu 22.04.3 LTS with an AMD EPYC 7742 64-core processor (1.5 GHz), 2 TiB of RAM, and a 1 TB SSD; the timeout was 5 min. We give the results in Table 1.

In the CORRECT scenario, we can see that with the exception of the BV-SING and GHZ-SING benchmarks (which are much easier because the precondition is a singleton set), AUTOQ outperforms other tools by several orders of magnitude and scales much better with increasing sizes of the circuits. Even on the two mentioned benchmarks, AUTOQ is still competitive; although slower than SLIQSIM, it still performs much better than SV-SIM (which fails due to running out of memory).

Comparing AUTOQ with the closest competitor, AUTOQ-OLD, which is based on traditional tree automata, we can see that the use of LSTAs in most cases yields a dramatic speed-up, affirming the usefulness of LSTAs. Neither SYMQV nor CAAL managed to finish on any of the benchmarks here.

In the MISSGATE and FLIPGATE scenarios, AUTOQ again outperforms AUTOQ-OLD by several orders of magnitude. Contrary to the T scenario, SYMQV and CAAL manage to finish on a few benchmarks (SYMQV: 1 benchmark in MISSGATE; CAAL: 3 benchmarks in MISSGATE and 4 benchmarks in FLIPGATE), successfully catching the bugs. The performance of AUTOQ is, however, still much better.

We also demonstrate the expressiveness of LSTA as a specification language and the versatility of AUTOQ by using it to check the equivalence of circuits. AUTOQ is not optimized for this task, and as expected, it is not as efficient as specialized circuit equivalence checkers such as SLIQC [17, 54] and QCEC [15], but it can still handle several practical cases. The largest case (in the number of qubits) we can handle is the circuit add64_164 from REVLIB [55], with 193 qubits and 256 gates before optimization. We used QISKIT [7] to transpile and optimize it and then check equivalence of the optimized circuit and the original one (cf. Section 4.3). AUTOQ was able to verify the equivalence between the two versions within 24 seconds.

We emphasize that the LSTA-based approach is the most efficient when the number of distinct amplitude values of reachable quantum states is small. For circuits such as the quantum Fourier transform (QFT), where the reachable quantum states have an exponential number of distinct amplitude values, our approach with the current state encoding struggles. A potential alternative encoding is discussed in Section 8.3.

8 Towards Parameterized Verification of Quantum Circuits

Let us now move to verification of *parameterized circuits*, i.e., checking correctness of a (typically) infinite family of quantum circuits with a similar structure (differing in the number of qubits). To the best of our knowledge, parameterized verification of quantum circuits has not been addressed by any fully automated approach so far. In this section, we will show that the use of LSTAs enables automated verification of a certain class of parameterized circuits. In particular, we will demonstrate how to use LSTAs to verify the parameterized GHZ circuit [29] and proceed to the verification of other circuits used in practice, such as circuits implementing parameterized *fermionic unitary evolution*. Our modelling and experiments with yet another class of parameterized circuits performing *diagonal Hamiltonian simulation* can be found in [2]. At the end, we will discuss the challenges and a direction towards a complete framework for parameterized circuit verification.

8.1 Verification of the Parameterized GHZ Circuit

An n -qubit *GHZ state* (for $n \geq 1$) is a state of the form $\frac{|0^n\rangle + |1^n\rangle}{\sqrt{2}}$ and an LSTA recognizing such states can be found in Fig. 20a. An n -qubit *GHZ circuit* is shown in Fig. 20b; it first executes the H_1 gate and then the sequence of gates $CX_2^1, CX_3^2, \dots, CX_n^{n-1}$. The number of CX gates involved is $n - 1$. The circuit transforms a quantum state of the form $|0^n\rangle$ (represented by the LSTA in Fig. 6) to $\frac{|0^n\rangle + |1^n\rangle}{\sqrt{2}}$ (represented by the LSTA in Fig. 20a). To execute this family of circuits, we need to support parameterized quantum gates, which is generally hard but still feasible in our framework for some cases. We first introduce the *parameterized CX(n) gate*, which implements the sequence of $n - 1$ CX gates on n qubits (cf. Figs. 20b and 20c). We will now describe how the effect of such a parameterized gate is computed on an LSTA representing a set of quantum states.

CX(n) gate In Algorithm 6, we introduce a procedure to build an LSTA $CX(n)(\mathcal{A})$ representing the set of states after executing the CX(n) gate on all qubits. Recall that the effect of applying the CX_{i+1}^i gate on a state has the same effect of applying an X^{i+1} gate on the 1-subtree below every

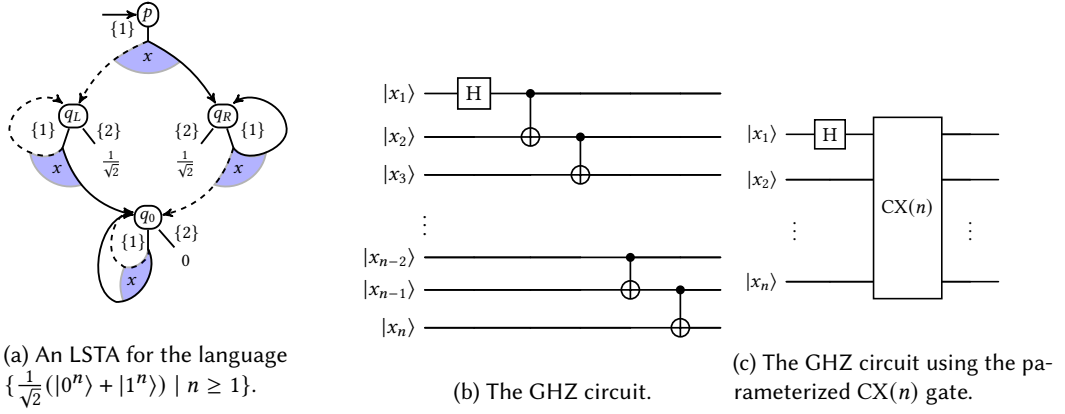


Fig. 20. An LSTA for the set of GHZ states (a), the GHZ circuit (b), and the parameterized $CX(n)$ gate (c). We note that in our uses of the $CX(n)$ gate (and other parameterized gates), the inputs are given by the order of qubits (i.e., corresponding to the schema in (b)).

node labeled x_i . Moreover, performing X gate to all qubits of a state, i.e., the $X^{\otimes n}$ gate, reverses the corresponding vector of amplitudes, e.g., from $(a, b, c, d)^T$ to $(d, c, b, a)^T$ or, equivalently, reverses all amplitude values of the tree. Thus, in Algorithm 6, we first construct a primed version $\overline{\mathcal{A}} = X^{\otimes n}(\mathcal{A})$, which encodes trees obtained by reversing the amplitude values of states in $\mathcal{L}(\mathcal{A})$. Such an LSTA $\overline{\mathcal{A}}$ can be constructed from \mathcal{A} by swapping the two bottom states of all non-leaf transitions (Lines 1–2). The resulting automaton is then obtained by combining \mathcal{A} and $\overline{\mathcal{A}}$ such that the right-hand bottom state of \mathcal{A} is reconnected to the corresponding state of $\overline{\mathcal{A}}$ (Line 3), i.e., jumping to $\overline{\mathcal{A}}$ when the control qubit has value 1, and the left-hand bottom state of $\overline{\mathcal{A}}$ is reconnected to the corresponding state of \mathcal{A} (Line 4), i.e., jumping back to the original LSTA when control qubit has value 0. Here, Δ_0 and $\overline{\Delta}_0$ are the sets of leaf transitions.

THEOREM 18. $\mathcal{L}(CX(n)(\mathcal{A})) = \{CX_n^{n-1}(\dots CX_2^1(T) \dots) \mid T \in \mathcal{L}(\mathcal{A})\}$ and $|CX(n)(\mathcal{A})| = 2|\mathcal{A}|$.

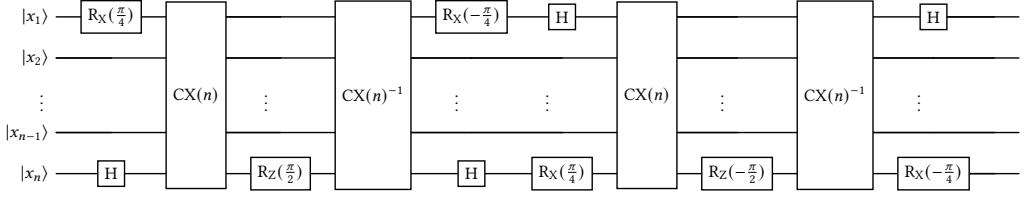
To verify the parameterized GHZ circuit, we begin by using the precondition P provided in the LSTA of Fig. 6. Next, we apply the H_1 operation using Algorithm 1 and reduce the output. We then run Algorithm 6 on this LSTA to obtain $\text{post}_C(P)$. Finally, we check for inclusion against the postcondition Q in Fig. 20a.

Non-parameterized gates Our construction of (non-parameterized) LSTA quantum gate operations from Section 5 targeting qubit x_t requires explicitly assigned index numbers to the first t qubits. We can obtain the explicit qubit numbering by *unfolding* the transitions for t layers from the root states and labeling them in order from x_1 to x_t .⁷ We can unfold the last qubit x_t using a similar construction. After applied a quantum gate, the LSTA can be *folded* again by replacing all indexed qubit symbols x_i with x and running a reduction algorithm.

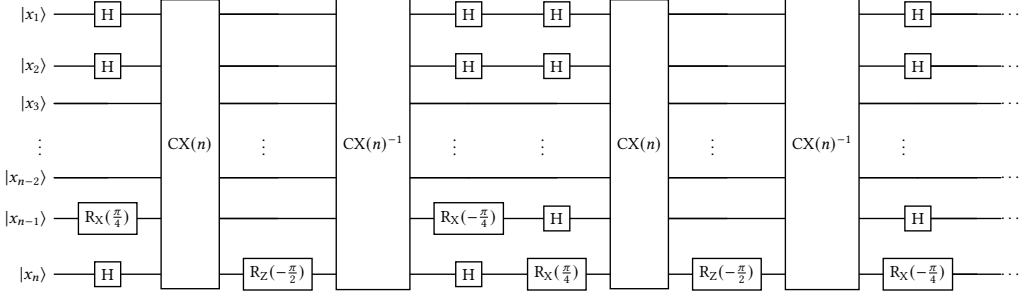
8.2 Verification of Fermionic Unitary Evolutions

Two major challenges in the practical realization of the *variational quantum eigensolver* on *noisy intermediate-scale quantum* (NISQ) computers are the design of *ansatz* states (i.e., states that serve

⁷One way to do this is to create t copies of the LSTA \mathcal{A} and name them \mathcal{A}_1 to \mathcal{A}_t . Next, we rename the transition symbols of \mathcal{A}_i from x to x_i and states from s to s_i for $1 \leq i \leq t$. After that, we connect these LSTAs and form an unfolded one. Starting from \mathcal{A}_1 , for each state s_1 that can be reached from root states in one step, we replace it with s_2 and thus jump to \mathcal{A}_2 . We then find a one-step reachable state from s_2 and jump to s_3 , and repeat this process until we jump from \mathcal{A}_t to \mathcal{A} .



(a) A standard circuit performing a single fermionic excitation.



(b) Part of the circuit performing a double fermionic excitation. See [59, Fig. 11] for the whole circuit.

Fig. 21. Circuits performing single and double fermionic excitations. The order of qubits for the $CX(n)$ and $CX(n)^{-1}$ gates correspond to the order of qubits in Figs. 20b and 22.

as the initial *guess* of the final value) and the construction of efficient circuits to prepare these states for a parameterized number of qubits. Most ansatz states considered by the quantum chemistry and material science communities correspond to applying a series of *fermionic unitary evolutions* to an initial reference state [59]. These evolutions are referred as single and double *fermionic excitations* and can be transformed via *Jordan-Wigner* encoding into the quantum circuits in Fig. 21a and Fig. 21b [59]. Note that the circuits use the parameterized $CX(n)^{-1}$ gate, which is given in Fig. 22 and whose implementation in our framework is given in Algorithm 7. Both circuits can be verified in our framework against the precondition $\{|0^n\rangle \mid n \geq 1\}$ (Fig. 6).

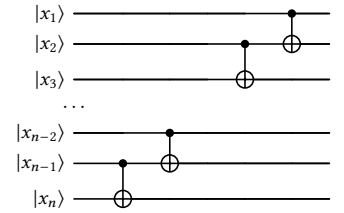


Fig. 22. The $CX(n)^{-1}$ gate.

Algorithm 6: Application of the $CX(n)$ gate on an LSTA

Input: An LSTA $\mathcal{A} = \langle Q, \Sigma, \Delta, \mathcal{R} \rangle$ representing a parameterized set of quantum states

Output: An LSTA $CX(n)(\mathcal{A})$

- 1 Build $\bar{\mathcal{A}} = \langle \bar{Q}, \Sigma, \bar{\Delta}, \bar{\mathcal{R}} \rangle$, a barred copy of \mathcal{A} with
 - 2 $\bar{\Delta} = \{\bar{q} \rightarrow c \mid f(\bar{q}_r, \bar{q}_l) \mid q \rightarrow c \mid f(q_l, q_r) \in \Delta\} \cup \{\bar{q} \rightarrow c \mid q \rightarrow c \mid c \in \Delta\}$; // $\bar{\mathcal{A}} = X^{\otimes n}(\mathcal{A})$
 - 3 $\Delta^R := \{q \rightarrow c \mid f(q_l, \bar{q}_r) \mid q \rightarrow c \mid f(q_l, q_r) \in \Delta\} \cup$
 - 4 $\{\bar{q} \rightarrow c \mid f(q_r, \bar{q}_l) \mid \bar{q} \rightarrow c \mid f(\bar{q}_r, \bar{q}_l) \in \bar{\Delta}\} \cup \Delta_0 \cup \bar{\Delta}_0$;
 - 5 **return** $\mathcal{A}^R = \langle Q \uplus \bar{Q}, \Sigma, \Delta^R, \mathcal{R} \rangle$;
-

Algorithm 7: Application of the $CX(n)^{-1}$ gate on an LSTA**Input:** An LSTA $\mathcal{A} = \langle Q, \Sigma, \Delta, \mathcal{R} \rangle$ representing a parameterized set of quantum states**Output:** An LSTA $CX(n)^{-1}(\mathcal{A})$

- 1 Build $\overline{\mathcal{A}} = \langle \overline{Q}, \Sigma, \overline{\Delta}, \overline{\mathcal{R}} \rangle$ with
- 2 $\overline{\Delta} = \{\overline{q} - C \rightarrow f(\overline{q}_r, \overline{q}_l) \mid q - C \rightarrow f(q_l, q_r) \in \Delta\} \cup \{\overline{q} - C \rightarrow c \mid q - C \rightarrow c \in \Delta\}; // \overline{\mathcal{A}} = X^{\otimes n}(\mathcal{A})$
- 3 $\Delta^R := \{q - C \rightarrow f(q_l, \overline{q}_r) \mid q - C \rightarrow f(q_l, q_r) \in \Delta\} \cup$
- 4 $\{\overline{q} - C \rightarrow f(\overline{q}_r, q_l) \mid \overline{q} - C \rightarrow f(\overline{q}_r, \overline{q}_l) \in \overline{\Delta}\} \cup \Delta_0 \cup \overline{\Delta}_0;$
- 5 **return** $\mathcal{A}^R = \langle Q \uplus \overline{Q}, \Sigma, \Delta^R, \mathcal{R} \rangle;$

CX(n)⁻¹ gate Algorithm 7 is very similar to Algorithm 6. The only difference between is that on Line 4, the right-hand bottom state of $\overline{\mathcal{A}}$ is reconnected to the corresponding state of \mathcal{A} , not the left-hand side state, i.e., we jump back to the original LSTA when the value of the control qubit is 1.

THEOREM 19. $\mathcal{L}(CX(n)^{-1}(\mathcal{A})) = \{CX_2^1(\dots CX_n^{n-1}(T) \dots) \mid T \in \mathcal{L}(\mathcal{A})\}$ and $|CX(n)^{-1}(\mathcal{A})| = 2|\mathcal{A}|$.

Other parameterized gates Our framework supports not only $CX(n)$ and $CX(n)^{-1}$ gates, but also $X^{\otimes n}$, $(D^{1, \omega_N^n})^{\otimes n}$, and some alternating patterns of CX gates. More details can be found in [2].

8.3 Evaluation and Discussion

We extended AUTOQ to support parameterized verification and used it to verify the circuits from Figs. 20c, 21a and 21b, and a circuit for diagonal Hamiltonian simulation (DHS; cf. [2]). The results are given in Table 2. All of these families of circuits could be verified efficiently. Even though the sets of encoded quantum states are infinitely large, their symbolic representation is compact (less than 10 states and 20 transitions).

Our current approach supports a limited set of parameterized quantum gates. Specifically, the gate $H^{\otimes n}$ is currently beyond our capability because applying it to the states $|0^n\rangle$ would create an infinite set of constant symbols $\{\frac{1}{\sqrt{2}^k} \mid k \in \mathbb{N}\}$. To overcome this challenge, we propose introducing a *state variable* s to represent the current basis state⁸ (i.e., the values of qubits on the branch in the tree) and using it in the leaf symbol. E.g., this would allow us to use the singleton set $\{\frac{1}{\sqrt{2}^{|s|}}\}$ as the leaf symbols, where $|s|$

represents the number of qubits. It also makes the leaf symbols after executing a *quantum Fourier transform* (QFT) circuit more concise. In the case of two qubits, QFT converts a quantum state $(a, b, c, d)^T$ to a tree with all leaves labeled with $(a + b\omega^{1 \cdot s} + c\omega^{2 \cdot s} + d\omega^{3 \cdot s})$, which can be made concise with the proposed encoding. We are quite enthusiastic about exploring this direction further in the future, as it promises to extend our approach's capabilities and open new possibilities for parameterized quantum circuit verification.

9 Related Work

We split the related works into two parts. First, we provide an overview of approaches of quantum circuits analysis and explain where our approach stands among existing tools. Then we will provide a detailed comparison of the quantum predicates we use and those of D'Hondt and Panangaden [24], which are used in the standard quantum Hoare logic of Ying [58].

⁸A similar concept of using state variables is utilized in the path-sum approach [6, 16].

Table 2. Results for the verification of parameterized circuits

	#G	AUTOQ		
		post _C	⊆	total
Fig. 20c	2	0.0s	0.0s	0.0s
DHS	4	0.0s	0.0s	0.0s
Fig. 21a	14	0.3s	0.0s	0.3s
Fig. 21b	88	1m54s	0.0s	1m54s

9.1 Approaches for Quantum Circuit Analysis

In recent years, many techniques for analyzing, simulating, and verifying quantum circuits and programs have emerged in the formal methods community.

Symbolic Quantum Circuit Verifiers: As mentioned in the introduction, these tools are fully automated, flexible in specifying verification properties, and provide precise bug traces. The closest work to ours is [18, 19], which uses traditional tree automata [23] to encode predicates representing sets of quantum states. We use the same verification framework as in [18, 19], employing automata to specify pre- and post-conditions and developing algorithms for the symbolic execution of quantum gates. LSTAs solve the scalability issues in many cases where the size of the representation using traditional TAs blew up (cf. Section 7), due to the introduction of level synchronization. Moreover, our single qubit gate operations are quadratic, while those of [18, 19] are exponential. There are two more tools that belong to this category: symQV [9] is based on *symbolic execution* [34] to verify input-output relationship with queries discharged by SMT solvers over the theory of reals. The SMT array theory approach [20] improved the previous by allowing a polynomial-sized circuit encoding but still faces a similar scalability problem. As we can see from our experiments, AUTOQ significantly outperforms all of the above tools in this category by several orders of magnitude. Another scalable fully automated approach for analysis of quantum circuits is *quantum abstract interpretation* [46, 60]. Our approach is more suitable for bug hunting as it does not rely on overapproximation, which is used by quantum abstract interpretation.

Deductive quantum circuit/program verifiers: These tools allow the verification of quantum programs w.r.t. very expressive specification languages (to be discussed in the next part). One most prominent family of approaches is based on the so-called *quantum Hoare logic* [26, 38, 51, 58, 61]. These approaches, however, require significant manual work and user expertise (they are often based on the use of interactive theorem provers such as ISABELLE [45] and CoQ [11]). The approach implemented in QBRICKS [16] tries to alleviate this issue by generating proof obligations and discharging them automatically using SMT solvers, but this still requires a lot of interaction with the user (e.g., when verifying Grover’s search for an arbitrary number of qubits, the experiment needed over one hundred user interactions).

Quantum circuit equivalence checkers: These tools are usually fully automated but are limited to only checking equivalence of two circuits. In contrast, our approach is flexible in specifying custom properties. Equivalence checkers are based on several approaches. One approach is based on the *ZX-calculus* [22], which is a graphical language used for reasoning about quantum circuits. The *path-sum* approach (implemented, e.g., within the tool FEYNMAN [6]) uses rewrite rules. Pre-computed equivalence sets are used to prove equivalence in QUARTZ [57]. QCEC [15] is an equivalence checker that uses decision diagrams and ZX-calculus, and SLIQEC [17, 54] also uses decision diagrams for (partial) equivalence checking. An approach based on working with the so-called *stabilizer states* [49] can be used to verify the equivalence of circuits with Clifford gates in polynomial time.

Quantum circuit simulators: Simulators can be categorized into decision diagram-based [41, 48, 50, 62], vector-based [37], and tensor-network-based [39, 52]. These simulators are designed to compute the circuit output for a single input state. They can also be used to verify the behavior of quantum circuits for a finite number of input states by simulating all. Our experiments, however, show that when preconditions permit exponentially many states, these simulators do not scale well to large numbers of qubits. Our approach can be viewed as a generalization of the decision diagram-based method, allowing us to handle sets of input states simultaneously. While tensor networks (TN) have proven highly efficient in simulations for physics applications and “quantum supremacy”

benchmarks, they have yet to be adapted for verification purposes. Investigating TN-based methods for verification presents a promising avenue for future research. In particular, exploring how TN simulation techniques, such as the decision diagram variant [31], could be extended to automata for verification is a compelling direction for future work.

9.2 Comparison with the Quantum Predicates of D’Hondt and Panangaden [24]

In the set-based approach ([18, 19] and this paper), a predicate maps a *pure state* to 0 or 1. Automata are used as compact representations of set-based predicates. A tree (representing a pure state) is accepted by an automaton iff the predicate maps the corresponding pure state to 1. On the other hand, in [24] and the quantum Hoare logic of Ying [58], a predicate is a mapping from a *mixed state* (a distribution over pure states) to a real value between 0 and 1, capturing the likelihood of mixed states satisfying the specified condition. An important advantage of the set-based approach is that it includes an efficient automated verification algorithm, whereas standard quantum Hoare logic typically relies on an interactive deductive method, requiring more manual effort. Furthermore, we demonstrate the potential of the set-based approach for automatic parameterized verification of quantum circuits.

The two type of predicates are incomparable in terms of expressive power. The predicates used in [24] are “continuous” in the sense that two “similar” mixed states (say, up to trace distance) will be mapped to two similar values. In contrast, our predicates are “discrete.” For two “similar” pure states, our predicates can map one to 1 and the other to 0. There are pros and cons of both systems. For instance, the “continuous” predicates [24, 58] can do a more fine-grained analysis of *quantum programs*⁹; they can talk about the probability of a pure state at the output. They can also talk about the expected value of a certain observation. In contrast, the “discrete” predicate can only verify state non-zero reachability, but not the precise probability. Conversely, continuous predicates cannot precisely describe discrete sets of states or vectors due to their continuous nature. Discrete predicates can specify the identity of a circuit (and thus circuit equivalence) using a set of 2^n linearly independent vectors simultaneously as the pre- and post-conditions (cf. Section 4), encoded with a linear number of transitions relative to n . It might seem natural to represent a set of pure states $\{|\phi_i\rangle \mid 0 \leq i \leq n\}$ by summing their outer products, $\sum_{0 \leq i \leq n} |\phi_i\rangle \langle \phi_i|$, and use this as a predicate in Ying’s quantum Hoare logic [58]. However, doing so can lead to ambiguity, as different sets of pure states may correspond to the same predicate. For instance, the sets $\{|0\rangle, |1\rangle\}$ and $\{|-\rangle, |+\rangle\}$ ¹⁰ yield the same outer product sum, failing to distinguish between distinct pure states.

Nevertheless, the “continuous” predicates are not necessarily incompatible with the proposed LSTA model. Using LSTAs to automate the reasoning over quantum program against “continuous” predicates would be an interesting and fruitful research direction.

Data Availability Statement

An environment with the tools and data used for the experimental evaluation in the current study is available at [1].

Acknowledgements

We thank Mingsheng Ying for his insightful comments and suggestions on the potential of using automata to automate the reasoning based on “continuous” predicates. Moreover, we thank the anonymous reviewers for their feedback that helped to improve the quality of the paper. This work was supported by the Czech Ministry of Education, Youth and Sports ERC.CZ project LL1908, the

⁹Quantum programs are an extension of quantum circuits that allows branching and loop statements.

¹⁰ $|+\rangle = \frac{1}{\sqrt{2}}(|0\rangle + |1\rangle)$ and $|-\rangle = \frac{1}{\sqrt{2}}(|0\rangle - |1\rangle)$

Czech Science Foundation project 23-07565S, the FIT BUT internal project FIT-S-23-8151, National Science and Technology Council, R.O.C., projects NSTC-112-2222-E-001-002-MY3, NSTC-113-2119-M-001-009, and NSTC-113-2222-E-027-007, ASOFR (Air Force Office of Scientific Research) project FA2386-23-1-4107, Foxconn research project 05T-1120327-1C, the Academia Sinica Grand Challenge Seeding Project AS-GCS-113-M06, the Academia Sinica Investigator Project Grant AS-IV-114-M07, and The Swedish Research Council.

References

- [1] Parosh Aziz Abdulla, Yo-Ga Chen, Yu-Fang Chen, Lukáš Holík, Ondřej Lengál, Fang-Yi Lo Jyun-Ao Lin, and Wei-Lun Tsai. 2024. *Verifying Quantum Circuits with Level-Synchronized Tree Automata (artifact)*. <https://doi.org/10.5281/zenodo.13957472> <https://doi.org/10.5281/zenodo.13957472>
- [2] Parosh Aziz Abdulla, Yo-Ga Chen, Yu-Fang Chen, Lukáš Holík, Ondřej Lengál, Jyun-Ao Lin, Fang-Yi Lo, and Wei-Lun Tsai. [n.d.]. *Verifying Quantum Circuits with Level-Synchronized Tree Automata (Technical Report)*. arXiv:2410.18540 [cs.LO] <https://arxiv.org/abs/2410.18540> <https://arxiv.org/abs/2410.18540>
- [3] Parosh Aziz Abdulla, Johanna Högberg, and Lisa Kaati. 2007. Bisimulation Minimization of Tree Automata. *Int. J. Found. Comput. Sci.* 18, 4 (2007), 699–713. <https://doi.org/10.1142/S0129054107004929>
- [4] Parosh Aziz Abdulla, Bengt Jonsson, Marcus Nilsson, and Mayank Saksena. 2004. A survey of regular model checking. In *International Conference on Concurrency Theory*. Springer, 35–48.
- [5] Thorsten Altenkirch and Jonathan Grattage. 2005. A Functional Quantum Programming Language. In *20th IEEE Symposium on Logic in Computer Science (LICS 2005), 26-29 June 2005, Chicago, IL, USA, Proceedings*. IEEE Computer Society, 249–258. <https://doi.org/10.1109/LICS.2005.1>
- [6] Matthew Amy. 2018. Towards Large-scale Functional Verification of Universal Quantum Circuits. In *Proceedings 15th International Conference on Quantum Physics and Logic, QPL 2018, Halifax, Canada, 3-7th June 2018 (EPTCS, Vol. 287)*, Peter Selinger and Giulio Chiribella (Eds.). 1–21. <https://doi.org/10.4204/EPTCS.287.1>
- [7] MD SAJJID ANIS, Abby-Mitchell, Héctor Abraham, et al. 2021. Qiskit: An Open-source Framework for Quantum Computing. <https://doi.org/10.5281/zenodo.2573505>
- [8] Frank Arute et al. 2019. Quantum supremacy using a programmable superconducting processor. *Nature* 574, 7779 (Oct. 2019), 505–510. <https://doi.org/10.1038/s41586-019-1666-5> Number: 7779 Publisher: Nature Publishing Group.
- [9] Fabian Bauer-Marquart, Stefan Leue, and Christian Schilling. 2023. symQV: Automated Symbolic Verification of Quantum Programs. In *Formal Methods - 25th International Symposium, FM 2023, Lübeck, Germany, March 6-10, 2023, Proceedings (Lecture Notes in Computer Science, Vol. 14000)*, Marsha Chechik, Joost-Pieter Katoen, and Martin Leucker (Eds.). Springer, 181–198. https://doi.org/10.1007/978-3-031-27481-7_12
- [10] Ethan Bernstein and Umesh V. Vazirani. 1993. Quantum complexity theory. In *Proceedings of the Twenty-Fifth Annual ACM Symposium on Theory of Computing, May 16-18, 1993, San Diego, CA, USA, S. Rao Kosaraju, David S. Johnson, and Alok Aggarwal (Eds.)*. ACM, 11–20. <https://doi.org/10.1145/167088.167097>
- [11] Yves Bertot and Pierre Castéran. 2013. *Interactive theorem proving and program development: Coq’Art: the calculus of inductive constructions*. Springer Science & Business Media.
- [12] Jacob D. Biamonte, Peter Wittek, Nicola Pancotti, Patrick Rebentrost, Nathan Wiebe, and Seth Lloyd. 2017. Quantum machine learning. *Nature* 549, 7671 (2017), 195–202. <https://doi.org/10.1038/nature23474>
- [13] Bruno Bogaert and Sophie Tison. 1992. Equality and Disequality Constraints on Direct Subterms in Tree Automata. In *STACS 92, 9th Annual Symposium on Theoretical Aspects of Computer Science, Cachan, France, February 13-15, 1992, Proceedings (Lecture Notes in Computer Science, Vol. 577)*, Alain Finkel and Matthias Jantzen (Eds.). Springer, 161–171. https://doi.org/10.1007/3-540-55210-3_181
- [14] Ahmed Bouajjani, Peter Habermehl, Adam Rogalewicz, and Tomáš Vojnar. 2012. Abstract regular (tree) model checking. *International Journal on Software Tools for Technology Transfer* 14, 2 (2012), 167–191. <https://doi.org/10.1007/s10009-011-0205-y>
- [15] Lukas Burgholzer and Robert Wille. 2020. Advanced equivalence checking for quantum circuits. *IEEE Transactions on Computer-Aided Design of Integrated Circuits and Systems* 40, 9 (2020), 1810–1824. <https://doi.org/10.1109/TCAD.2020.3032630>
- [16] Christophe Chareton, Sébastien Bardin, François Bobot, Valentin Perrelle, and Benoît Valiron. 2021. An Automated Deductive Verification Framework for Circuit-Building Quantum Programs. In *ESOP (LNCS, Vol. 12648)*, Nobuko Yoshida (Ed.). Springer International Publishing, Cham, 148–177. https://doi.org/10.1007/978-3-030-72019-3_6
- [17] Tian-Fu Chen, Jie-Hong R. Jiang, and Min-Hsiu Hsieh. 2022. Partial Equivalence Checking of Quantum Circuits. In *IEEE International Conference on Quantum Computing and Engineering, QCE 2022, Broomfield, CO, USA, September 18-23, 2022*. IEEE, 594–604. <https://doi.org/10.1109/QCE53715.2022.00082>

- [18] Yu-Fang Chen, Kai-Min Chung, Ondrej Lengál, Jyun-Ao Lin, and Wei-Lun Tsai. 2023. AutoQ: An Automata-Based Quantum Circuit Verifier. In *Computer Aided Verification - 35th International Conference, CAV 2023, Paris, France, July 17-22, 2023, Proceedings, Part III (Lecture Notes in Computer Science, Vol. 13966)*, Constantin Enea and Akash Lal (Eds.). Springer, 139–153. https://doi.org/10.1007/978-3-031-37709-9_7
- [19] Yu-Fang Chen, Kai-Min Chung, Ondrej Lengál, Jyun-Ao Lin, Wei-Lun Tsai, and Di-De Yen. 2023. An Automata-Based Framework for Verification and Bug Hunting in Quantum Circuits. *Proc. ACM Program. Lang.* 7, PLDI (2023), 1218–1243. <https://doi.org/10.1145/3591270>
- [20] Yu-Fang Chen, Philipp Rümmer, and Wei-Lun Tsai. 2023. A Theory of Cartesian Arrays (with Applications in Quantum Circuit Verification). In *International Conference on Automated Deduction*. Springer, 170–189.
- [21] Carlo Ciliberto, Mark Herbster, Alessandro Davide Ialongo, Massimiliano Pontil, Andrea Rocchetto, Simone Severini, and Leonard Wossnig. 2018. Quantum Machine Learning: A Classical Perspective. *Proceedings of the Royal Society A: Mathematical, Physical and Engineering Sciences* 474, 2209 (January 2018). <https://doi.org/10.1098/rspa.2017.0551>
- [22] Bob Coecke and Ross Duncan. 2011. Interacting quantum observables: categorical algebra and diagrammatics. *New Journal of Physics* 13, 4 (apr 2011), 043016. <https://doi.org/10.1088/1367-2630/13/4/043016>
- [23] Hubert Comon, Max Dauchet, Rémi Gilleron, Florent Jacquemard, Denis Lugiez, Christof Löding, Sophie Tison, and Marc Tommasi. 2008. Tree automata techniques and applications.
- [24] Ellie D'Hondt and Prakash Panangaden. 2006. Quantum weakest preconditions. *Mathematical Structures in Computer Science* 16, 3 (2006), 429–451.
- [25] Javier Esparza and Michael Blondin. 2023. *Automata Theory: An Algorithmic Approach*. MIT Press.
- [26] Yuan Feng and Mingsheng Ying. 2021. Quantum Hoare logic with classical variables. *ACM Transactions on Quantum Computing* 2, 4 (2021), 1–43. <https://doi.org/10.1145/3456877>
- [27] Emmanuel Filiot, Jean-Marc Talbot, and Sophie Tison. 2010. Tree Automata with Global Constraints. *Int. J. Found. Comput. Sci.* 21, 4 (2010), 571–596. <https://doi.org/10.1142/S012905411000743X>
- [28] Alexander S. Green, Peter LeFanu Lumsdaine, Neil J. Ross, Peter Selinger, and Benoît Valiron. 2013. Quipper: a scalable quantum programming language. In *ACM SIGPLAN Conference on Programming Language Design and Implementation, PLDI '13, Seattle, WA, USA, June 16-19, 2013*, Hans-Juergen Boehm and Cormac Flanagan (Eds.). ACM, 333–342. <https://doi.org/10.1145/2491956.2462177>
- [29] Daniel M. Greenberger, Michael A. Horne, and Anton Zeilinger. 1989. Going Beyond Bell's Theorem. In *Bell's Theorem, Quantum Theory and Conceptions of the Universe*, Menas Kafatos (Ed.). Springer Netherlands, Dordrecht, 69–72. https://doi.org/10.1007/978-94-017-0849-4_10
- [30] Lov K. Grover. 1996. A Fast Quantum Mechanical Algorithm for Database Search. In *Proceedings of the Twenty-Eighth Annual ACM Symposium on the Theory of Computing, Philadelphia, Pennsylvania, USA, May 22-24, 1996*, Gary L. Miller (Ed.). ACM, 212–219. <https://doi.org/10.1145/237814.237866>
- [31] Xin Hong, Xiangzhen Zhou, Sanjiang Li, Yuan Feng, and Mingsheng Ying. 2022. A Tensor Network based Decision Diagram for Representation of Quantum Circuits. *ACM Trans. Design Autom. Electr. Syst.* 27, 6 (2022), 60:1–60:30. <https://doi.org/10.1145/3514355>
- [32] Florent Jacquemard, Francis Klay, and Camille Vacher. 2009. Rigid Tree Automata. In *Language and Automata Theory and Applications, Third International Conference, LATA 2009, Tarragona, Spain, April 2-8, 2009. Proceedings (Lecture Notes in Computer Science, Vol. 5457)*, Adrian-Horia Dediu, Armand-Mihai Ionescu, and Carlos Martín-Vide (Eds.). Springer, 446–457. https://doi.org/10.1007/978-3-642-00982-2_38
- [33] Florent Jacquemard, Francis Klay, and Camille Vacher. 2011. Rigid tree automata and applications. *Inf. Comput.* 209, 3 (2011), 486–512. <https://doi.org/10.1016/J.IC.2010.11.015>
- [34] James C. King. 1976. Symbolic Execution and Program Testing. *Commun. ACM* 19, 7 (1976), 385–394. <https://doi.org/10.1145/360248.360252>
- [35] Florent Kirchner, Nikolai Kosmatov, Virgile Prevosto, Julien Signoles, and Boris Yakobowski. 2015. Frama-C: A software analysis perspective. *Formal aspects of computing* 27 (2015), 573–609.
- [36] K Rustan M Leino. 2010. Dafny: An automatic program verifier for functional correctness. In *International conference on logic for programming artificial intelligence and reasoning*. Springer, 348–370.
- [37] Ang Li and Sriram Krishnamoorthy. 2021. SV-Sim: Scalable PGAS-based State Vector Simulation of Quantum Circuits. In *Proceedings of the International Conference for High Performance Computing, Networking, Storage and Analysis*.
- [38] Junyi Liu, Bohua Zhan, Shuling Wang, Shenggang Ying, Tao Liu, Yangjia Li, Mingsheng Ying, and Naijun Zhan. 2019. Formal verification of quantum algorithms using quantum Hoare logic. In *International conference on computer aided verification*. Springer, 187–207. https://doi.org/10.1007/978-3-030-25543-5_12
- [39] Igor L Markov and Yaoyun Shi. 2008. Simulating quantum computation by contracting tensor networks. *SIAM J. Comput.* 38, 3 (2008), 963–981.
- [40] Sam McArdle, Suguru Endo, Alán Aspuru-Guzik, Simon C. Benjamin, and Xiao Yuan. 2020. Quantum computational chemistry. *Rev. Mod. Phys.* 92 (Mar 2020), 015003. Issue 1. <https://doi.org/10.1103/RevModPhys.92.015003>

- [41] D. Michael Miller and Mitchell A. Thornton. 2006. QMDD: A Decision Diagram Structure for Reversible and Quantum Circuits. In *36th IEEE International Symposium on Multiple-Valued Logic (ISMVL 2006)*, 17-20 May 2006, Singapore. IEEE Computer Society, 30. <https://doi.org/10.1109/ISMVL.2006.35>
- [42] Nikolaj Moll, Panagiotis Barkoutsos, Lev S Bishop, Jerry M Chow, Andrew Cross, Daniel J Egger, Stefan Filipp, Andreas Fuhrer, Jay M Gambetta, Marc Ganzhorn, Abhinav Kandala, Antonio Mezzacapo, Peter Müller, Walter Riess, Gian Salis, John Smolin, Ivano Tavernelli, and Kristan Temme. 2018. Quantum optimization using variational algorithms on near-term quantum devices. *Quantum Science and Technology* 3, 3 (jun 2018), 030503. <https://doi.org/10.1088/2058-9565/aab822>
- [43] P. Müller, M. Schwerhoff, and A. J. Summers. 2016. Automatic Verification of Iterated Separating Conjunctions using Symbolic Execution. In *Computer Aided Verification (CAV) (LNCS, Vol. 9779)*, S. Chaudhuri and A. Farzan (Eds.). Springer-Verlag, 405–425. http://link.springer.com/chapter/10.1007/978-3-319-41528-4_22
- [44] Michael A. Nielsen and Isaac L. Chuang. 2011. *Quantum Computation and Quantum Information: 10th Anniversary Edition* (10th ed.). Cambridge University Press, USA.
- [45] Tobias Nipkow, Lawrence C Paulson, and Markus Wenzel. 2002. *Isabelle/HOL: a proof assistant for higher-order logic*. Vol. 2283. Springer Science & Business Media.
- [46] Simon Perdrix. 2008. Quantum entanglement analysis based on abstract interpretation. In *International Static Analysis Symposium*. Springer, 270–282. https://doi.org/10.1007/978-3-540-69166-2_18
- [47] Helmut Seidl and Andreas Reuß. 2012. Extending \mathcal{H}_1 -Clauses with Path Disequalities. In *Foundations of Software Science and Computational Structures - 15th International Conference, FOSSACS 2012, Held as Part of the European Joint Conferences on Theory and Practice of Software, ETAPS 2012, Tallinn, Estonia, March 24 - April 1, 2012. Proceedings (Lecture Notes in Computer Science, Vol. 7213)*, Lars Birkedal (Ed.). Springer, 165–179. https://doi.org/10.1007/978-3-642-28729-9_11
- [48] Meghana Sista, Swarat Chaudhuri, and Thomas W. Reps. 2023. Symbolic Quantum Simulation with Quasimodo. In *Computer Aided Verification - 35th International Conference, CAV 2023, Paris, France, July 17-22, 2023, Proceedings, Part III (Lecture Notes in Computer Science, Vol. 13966)*, Constantin Enea and Akash Lal (Eds.). Springer, 213–225. https://doi.org/10.1007/978-3-031-37709-9_11
- [49] Dimitrios Thanos, Tim Coopmans, and Alfons Laarman. 2023. Fast Equivalence Checking of Quantum Circuits of Clifford Gates. In *Automated Technology for Verification and Analysis - 21st International Symposium, ATVA 2023, Singapore, October 24-27, 2023, Proceedings, Part II (Lecture Notes in Computer Science, Vol. 14216)*, Étienne André and Jun Sun (Eds.). Springer, 199–216. https://doi.org/10.1007/978-3-031-45332-8_10
- [50] Yuan-Hung Tsai, Jie-Hong R. Jiang, and Chiao-Shan Jhang. 2021. Bit-Slicing the Hilbert Space: Scaling Up Accurate Quantum Circuit Simulation. In *58th ACM/IEEE Design Automation Conference, DAC 2021, San Francisco, CA, USA, December 5-9, 2021*. IEEE, 439–444. <https://doi.org/10.1109/DAC18074.2021.9586191>
- [51] Dominique Unruh. 2019. Quantum Hoare logic with ghost variables. In *2019 34th Annual ACM/IEEE Symposium on Logic in Computer Science (LICS)*. IEEE, 1–13. <https://doi.org/10.1109/LICS.2019.8785779>
- [52] Guifré Vidal. 2003. Efficient Classical Simulation of Slightly Entangled Quantum Computations. *Phys. Rev. Lett.* 91 (Oct 2003), 147902. Issue 14. <https://doi.org/10.1103/PhysRevLett.91.147902>
- [53] Lieuwe Vinkhuijzen, Thomas Grurl, Stefan Hillmich, Sebastiaan Brand, Robert Wille, and Alfons Laarman. 2023. Efficient Implementation of LIMDDs for Quantum Circuit Simulation. In *Model Checking Software - 29th International Symposium, SPIN 2023, Paris, France, April 26-27, 2023, Proceedings (Lecture Notes in Computer Science, Vol. 13872)*, Georgiana Caltais and Christian Schilling (Eds.). Springer, 3–21. https://doi.org/10.1007/978-3-031-32157-3_1
- [54] Chun-Yu Wei, Yuan-Hung Tsai, Chiao-Shan Jhang, and Jie-Hong R. Jiang. 2022. Accurate BDD-based unitary operator manipulation for scalable and robust quantum circuit verification. In *DAC '22: 59th ACM/IEEE Design Automation Conference, San Francisco, California, USA, July 10 - 14, 2022*, Rob Oshana (Ed.). ACM, 523–528. <https://doi.org/10.1145/3489517.3530481>
- [55] R. Wille, D. Große, L. Teuber, G. W. Dueck, and R. Drechsler. 2008. RevLib: An Online Resource for Reversible Functions and Reversible Circuits. In *Int'l Symp. on Multi-Valued Logic*. 220–225. <https://doi.org/10.1109/ISMVL.2008.43> RevLib is available at <http://www.revlib.org>.
- [56] Robert Wille, Rod Van Meter, and Yehuda Naveh. 2019. IBM's Qiskit Tool Chain: Working with and Developing for Real Quantum Computers. In *Design, Automation & Test in Europe Conference & Exhibition, DATE 2019, Florence, Italy, March 25-29, 2019*, Jürgen Teich and Franco Fummi (Eds.). IEEE, 1234–1240. <https://doi.org/10.23919/DATE.2019.8715261>
- [57] Mingkuan Xu, Zikun Li, Oded Padon, Sina Lin, Jessica Pointing, Auguste Hirth, Henry Ma, Jens Palsberg, Alex Aiken, Umut A Acar, et al. 2022. Quartz: superoptimization of Quantum circuits. In *Proceedings of the 43rd ACM SIGPLAN International Conference on Programming Language Design and Implementation*. 625–640. <https://doi.org/10.1145/3519939.3523433>
- [58] Mingsheng Ying. 2012. Floyd-Hoare logic for quantum programs. *ACM Transactions on Programming Languages and Systems (TOPLAS)* 33, 6 (2012), 1–49. <https://doi.org/10.1145/2049706.2049708>

- [59] Yordan S. Yordanov, David R. M. Arvidsson-Shukur, and Crispin H. W. Barnes. 2020. Efficient quantum circuits for quantum computational chemistry. *Phys. Rev. A* 102 (Dec 2020), 062612. Issue 6. <https://doi.org/10.1103/PhysRevA.102.062612>
- [60] Nengkun Yu and Jens Palsberg. 2021. Quantum abstract interpretation. In *Proceedings of the 42nd ACM SIGPLAN International Conference on Programming Language Design and Implementation*. 542–558. <https://doi.org/10.1145/3453483.3454061>
- [61] Li Zhou, Nengkun Yu, and Mingsheng Ying. 2019. An applied quantum Hoare logic. In *Proceedings of the 40th ACM SIGPLAN Conference on Programming Language Design and Implementation*. 1149–1162. <https://doi.org/10.1145/3314221.3314584>
- [62] Alwin Zulehner and Robert Wille. 2019. Advanced Simulation of Quantum Computations. *IEEE Trans. Comput. Aided Des. Integr. Circuits Syst.* 38, 5 (2019), 848–859. <https://doi.org/10.1109/TCAD.2018.2834427>

Received 2024-07-11; accepted 2024-11-07